NASA TN D-1109

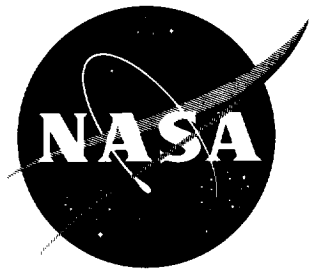

TECHNICAL NOTE

D-1109

INVESTIGATION OF THE PERFORMANCE OF AN AXIAL-FLOW-PUMP STAGE DESIGNED BY THE BLADE-ELEMENT THEORY - BLADE-ELEMENT DATA

By James E. Crouse, Richard F. Soltis, and John C. Montgomery

Lewis Research Center
Cleveland, Ohio

NATIONAL AERONAUTICS AND SPACE ADMINISTRATION

WASHINGTON

December 1961

NATIONAL AERONAUTICS AND SPACE ADMINISTRATION

TECHNICAL NOTE D-1109

INVESTIGATION OF THE PERFORMANCE OF AN AXIAL-FLOW-PUMP STAGE DESIGNED BY THE BLADE-ELEMENT THEORY - BLADE-ELEMENT DATA

By James E. Crouse, Richard F. Soltis, and John C. Montgomery

SUMMARY

An axial-flow-pump stage was designed by utilizing blade-element methods in conjunction with axial-flow-compressor blade-element theory. This report presents the blade-element data of the pump stage in both the noncavitating and cavitating conditions. The noncavitating blade-element performance is compared with design rules. The results indicated that some modification of the compressor design equations for computing minimum-loss incidence and deviation angles may be necessary for application to an axial-flow-pump design. Minimum values of observed rotor loss were slightly lower than anticipated from compressor results. At the design flow coefficient the rotor-blade elements were not operating at the reference incidence angles, and the experimental efficiency was lower than the design value. The observed head rise was very close to the design. An attempt was made to estimate the potential of this rotor by using the minimum measured values of loss coefficient and observed energy input at the design flow.

Performance of the pump at a suction specific speed of approximately 13,000 (cavitation number $k \approx 0.12$) showed only a slight dropoff in performance in the cavitation inception region from the noncavitating results. The observed performance at a suction specific speed of approximately 16,000 ($k \approx 0.09$) is also presented for comparison.

INTRODUCTION

The anticipated higher efficiency and better staging characteristic of the multistage axial-flow pump (as compared with the centrifugal-type pump) may make it particularly suitable for certain applications where high performance is desirable. As a first step in determining what performance levels can be achieved, an axial-flow-pump stage was designed at NASA and tested in the Lewis water tunnel. Since performance data from this type pump are very meager, the pump design utilized the mass of performance results accumulated from low-speed rotors and cascades

operated in air. The blade-element design approach was used with limitations on blade loading and empirical blade design equations developed for axial-flow compressors. The results of this investigation should then partially determine if the mass of data that was collected from cascade and compressor tests and developed into a design system is applicable to axial-flow-pump design.

A multistage axial-flow pump may be considered to be composed of a combination of three types of stages, namely:

(1) An inducer or a rotor that operates with various degrees of cavitation. Its purpose is to supply sufficient head rise to limit or prevent cavitation from occurring in succeeding stages.

(2) An inlet-type stage in which small amounts of cavitation could occur and in which the effects of loading and cavitation on the performance parameters of the blade row are interrelated.

(3) A pressure stage where the head rise is limited by loading alone. The stage reported herein could conceivably apply to either of the latter two categories listed previously. As a pressure stage only the design and overall performance is presented in reference 1. The results presented herein probe more deeply into the stage performance by presenting the radial distribution of performance across selected blade elements at varied flow conditions in both noncavitating and cavitating environments. In addition, the measured performance provides an initial evaluation of the usefulness of compressor design theory and data.

PUMP DESIGN

General Design Concepts

The pump stage for this investigation was designed by the blade-element methods and limitations of reference 2. The design was achieved in two major steps. First, the vector diagrams were established at several radii ahead of and behind each blade row. Second, a blade was specified to establish the design vector diagrams. A more complete discussion of the blade design concepts is given in reference 1. However, since the observed blade-element performance offers an opportunity to evaluate the design concepts, most of the design philosophy is repeated in the next section.

Rotor Design

Selection of vector diagrams. - An optimization procedure similar to the one reported in reference 3 was instrumental in determining the inlet vector diagrams since the rotor, when operated as an inlet-type

stage, could be expected to operate with some cavitation. Using this procedure resulted in a tip inlet relative flow angle of 73.6° for the selected conditions of a suction specific speed of 10,000, a 0.4 hub-tip ratio, and inlet axial flow. The inlet velocity was assumed constant in magnitude and axial in direction at all radii. This velocity distribution assumption and the inlet tip relative flow angle are sufficient information to establish the inlet velocity diagrams at all radii. The resulting ideal design flow coefficient φ_i (neglecting boundary-layer correction) was 0.293. By allowing a 3-percent boundary-layer correction the design operating φ becomes 0.284.

The rotor-outlet velocity diagrams are evolved from the desired radial distributions of either actual or ideal head rise (energy addition) and loss. The level of energy addition was set on the basis of blade loading. In axial-flow compressors a blade diffusion factor D defined as

$$D = \frac{V_1' - V_2'}{V_1'} + \frac{\Delta V_\theta'}{2\sigma V_1'}$$

for equal inlet and outlet blade-element radii was used as a measure of blade loading. (Symbols are defined in appendix A.) In compressors, a correlation of D factor with loss indicates that blade-element losses increased at a rapid rate as the D factor was increased above 0.45 in the rotor tip region and above 0.60 at all other blade elements. The same loading limits were applied to this pump design, and the initial values of loss used in the design were also estimated from the previous correlation.

The interrelation of the energy addition, loss, and D factor noted previously makes it necessary to use an iterative process to establish the outlet vector diagrams. A preliminary calculation based on the assumption of radially constant energy addition and losses and simplified radial equilibrium

$$\frac{dh}{dr} = \frac{V_\theta^2}{gr}$$

indicated that the limiting D factor was reached at the hub first. The corresponding D factor at the blade tip was approximately 0.25. Because the blade-element losses, as determined from the correlations presented in reference 4, resulted in blade-element efficiencies close to 90 percent at all radii, a distribution of losses corresponding to efficiencies of 90 percent at all radii was used, for simplicity, in the final design calculations. The resulting head coefficient was 0.146 at all radii. To obtain an overall value for the performance parameters of head rise and efficiency from the calculated blade-element values, it

would seem logical that a correction factor to account for the adverse effects of casing boundary layers should be applied (see ref. 2). However, since no precedent for the application of such a correction factor is known, the calculated blade-element values are used herein as the design values.

Selection of blading. - The next step is the selection of a blade to achieve the design vector diagrams. Considerable axial-flow compressor experimental data are available for the 65 series and double-circular-arc blade sections. Double-circular-arc blade sections were selected because of their sharp leading edges and simplicity. The blade incidence and deviation angles were calculated from the equations of reference 2 with the following modification. The design incidence and deviation angles used were the incidence and deviation angles computed from the correlation of low-speed cascade data ($i_{2\text{-}D}$ and $\delta_{2\text{-}D}$ in ref. 2, respectively). The blade nomenclature is shown in figure 1, and the specifications are listed in table I. The blade sections were stacked so that their centers of gravity were on a radial line. A photograph of the rotor is shown in figure 2.

Stator Design

In multistage pumps the purpose of the stator blade row is to set up the desired inlet flow conditions for the following rotor. For continuation of the type of rotor reported herein the stators should turn the flow back to the axial direction; however, the large amounts of turning required indicate that high blade loadings may be encountered in doing this. The blade diffusion factor with an approximate limiting value of 0.6 at all radii was used as the stator loading parameter.

It is necessary to use an iterative process to establish the stator-outlet velocity diagrams since the radial equilibrium, loss distribution, and D factor are interrelated. A preliminary calculation based on the assumption of constant losses showed that turning back to the axial direction could be achieved within these D factor limitations. Since the losses associated with these D factors as calculated from reference 2 were small, for simplicity the loss distribution was assumed constant across the stators in the finalized design. The resulting velocity distribution is axial and constant radially. Double-circular-arc blade sections were also used in the stators. The blade section incidence and deviation angles were determined from the design rules of reference 2. The stator-blade specifications are listed in table I.

APPARATUS AND PROCEDURE

Test Facility

Since the pump installation, instrumentation, and data-taking procedures are described in great detail in reference 1, they are discussed only briefly in this report. The pump was tested in the Lewis water tunnel, which is shown schematically in figure 3. The major components are shown in the diagram. An auxiliary system to the loop consists of degasifying and filtering units. The degasification unit is capable of reducing the gas content of the water to 1 part per million by weight. The gas content was maintained below 3 parts per million for the tests. The filtering system takes out solid matter larger than 5 microns.

Instrumentation

The instrumentation can be divided into two groups: (1) the instrumentation used to obtain overall test loop or general conditions and (2) the survey instruments for obtaining blade-element data. The test loop instrumentation consists of a Venturi flowmeter, an electronic speed counter in conjunction with a magnetic pickup, an automatic water temperature control and recorder, and a pressure transducer to measure the loop pressure. The survey instruments, which are shown in figure 4, are a claw for measuring total head, a rake, which has 14 tubes equally spaced at intervals of about 1/12 inch, for measuring the circumferential variation of total head behind the stators, and a wedge for measuring static head. Each claw and wedge has a null-balancing stream-direction-sensitive element that automatically alines the probe to the direction of flow. A head calibration factor for each wedge static probe was determined in an air tunnel and applied to the measured static pressures in the water tunnel. A single claw and a wedge were used at measuring stations 1 inch ahead of the rotor and midway between the rotor and stators. The rake and a wedge, which was used to measure both static head and flow angle, were located 1 inch behind the stators. The total and static pressures from the probes were measured with pressure transducers and were recorded, along with angles and radial location, on paper tape in a self-balancing digital potentiometer. The circumferential variations of total pressure obtained by the wake rake were recorded on a multitube mercury manometer board. The level of pressure was then established by means of a high-pressure gage. In order to increase accuracy, pressure differences were measured wherever possible. The estimated accuracy of measurements is tabulated as follows:

Flow rate, Q	$\leq \pm 1.0$ Percent
Rotative speed, N	± 0.5 Percent
Heads (ΔH or absolute head)	$\leq \pm 1$ Ft
Flow angles, β	$\pm 0.5^{\circ}$

Characteristic performance curves were obtained by operating the rotor at constant N and H_{SV} over a range of throttle settings. The data were taken by surveying total and static heads and flow angles across the annulus at preprogrammed radial positions located at 6, 10, 30, 50, 70, 90, and 94 percent of passage height from the tip. The data presented were taken along characteristic curves for the following conditions:

Tip speed, U_t, ft/sec	Net positive suction head, H_{SV}, ft
153	115
123	115
123	45
123	33

Computations

The computational procedure is discussed in detail in reference 1, and the equations used in the computations are presented in appendix B. The only calculation not self-evident in the equations is the method of computing the stator-outlet total head and stator loss coefficient.

In the computation of stator-blade-element loss coefficient, two procedures were used. The methods varied only in the selection of a stator-outlet ideal total head (see appendix B). In the first procedure the total head measured at the rotor outlet (stator inlet) was used. Values of stator loss coefficient computed using this procedure showed undue scatter and inconsistencies; however, they do represent values of loss attributed to stator row in the overall efficiency calculations. Sources of scatter and inconsistencies probably lie in measurement errors at both axial stations and in the circumferential variation of total pressure at the rotor outlet. (Sizable variations in the static head measured from wall taps around the casing behind the rotor and stator

were noted.) Also, since the calculation of both stage and stator performance involves the difference of two absolute pressures, the inherent inaccuracies in the measuring devices are compounded.

The second procedure used an average free-stream total head at the stator outlet as the ideal total head. This average free-stream total head was obtained by arithmetically averaging the heads (constituting a single blade spacing) across the wake along a smooth curve connecting the free-stream values on the two sides of the wake (see fig. 5(a)). The values of loss coefficient obtained from this procedure showed considerably less scatter and more consistency in the observed trends.

Wherever the stator-blade wake was clearly defined, the second procedure described previously was used to compute stator loss coefficient. Figure 5(a) presents some examples of total head distributions measured by the wake rake and the curves used in the calculation of average free-stream heads. At the flow conditions where blade wakes are not readily identified, the values of loss coefficient computed using the first computational procedure are presented for comparison purposes. These latter values are shown as solid symbols on the performance curves. Figure 5(b) presents some examples of wake rake distributions where blade wakes are not easily identified.

Some measure of the reliability of the data is obtained by a comparison of the integrated mass flow at the rotor inlet and the rotor and stator outlets with the mass flow as determined by the Venturi meter. The integrated flows compared with the Venturi flows within ±1.5 percent at the rotor inlet and ±3 percent at the rotor and stator outlets. Assumptions used in the calculation procedure include (1) no inlet whirl ($V_{\theta,1} = 0$) and (2) representation of average flow conditions around the periphery by a single measurement.

Selection of Blade-Element Performance Parameters

The design objective in the blade-element approach is to select blade sections at various radial locations to produce the change in direction of fluid flow (turning angle) required by the velocity diagram with a minimum of total-pressure loss. For this application, turning angle (or deviation angle) and total-pressure loss are the basic parameters. For the inverse problem, analysis of blade row performance, additional parameters prove helpful. From the turning angle and flow coefficient, the ideal head coefficient is determined; and, when the latter is used in conjunction with the loss data, the efficiency and head rise coefficient are obtained. To aid in the analysis of blade-element losses, blade loading and cavitation number are included.

Accordingly, the blade-element characteristics selected for analysis and design application include:

(1) Incidence angle, i

(2) Outlet deviation angle, δ

(3) Relative total-pressure loss coefficient, $\bar{\omega}$

(4) Flow coefficient, φ

(5) Ideal head rise coefficient, $\psi_i = \frac{g \Delta H_i}{U_t^2}$

(6) Head rise coefficient, ψ

(7) Efficiency, η

(8) Diffusion factor, D (a blade loading parameter developed in ref. 4)

(9) Cavitation number, k (a measure of the static-pressure drop (velocity increase) that may occur around the blade before reaching fluid vapor pressure)

A blade element as used herein is the blade section described on a cylinder about the axis of rotation.

RESULTS AND DISCUSSION

In this presentation the noncavitating performance, both overall and blade element, will be discussed first followed by the performance under cavitating conditions. Both rotor and stator blade row performance are presented and discussed on an individual basis. The stage is a combination of rotor and stator. To supplement this measured performance, some visual observations made during the test will be discussed briefly.

It has been noted during early tests in the Lewis water tunnel that the first indication of cavitation, or formation of water vapor, occurs in the leakage flows through the tip clearances of the rotor blades. Reference 5 uses this cavitation phenomenon as a means of studying tip clearance flows. For this particular rotor, cavitation, or vapor formation in the blade clearance region, was first clearly discernible at a suction specific speed of approximately 6000. However, the inlet pressure required to maintain a suction specific speed of 6000 or lower was higher than desired for continuous operation using the rotor Lucite casing. As the inlet pressure was lowered until suction specific speeds on the order of 10,000 were reached, no obvious effects on the performance at the radius selected to represent blade tip performance (10 percent of passage height from outer wall) could be detected. Consequently, the

latter flow conditions have been presented herein as noncavitating flow. Although vapor formation in the vortex caused by tip clearance flow was visible, no sign of cavitation on the blade surfaces could be seen.

Noncavitating Performance

Overall performance. - In figure 6 the overall rotor and stage performance is presented as head rise coefficient and efficiency plotted as functions of flow coefficient. For comparative purposes design values are included. The overall performance of this rotor is discussed in detail in reference 1; consequently, only a few brief remarks concerning it will be made.

At the design flow coefficient ($\varphi = 0.284$) the rotor achieved a measured head rise coefficient ψ of 0.144 (design $\psi = 0.146$) at a hydrodynamic efficiency η of 84.5 percent, while the stage showed values of 0.135 and 80 percent for head coefficient and efficiency, respectively.

In the calculation of overall efficiency, the rotor ideal head rise ψ_i was obtained from two different sources. Primarily, the ideal head rise was obtained by mass-averaging the change of angular momentum experienced across the individual blade elements. This result was then checked against a value obtained from torquemeter measurements. From the maximum flow point to a flow coefficient of 0.267, these trends compared favorably. During operation at flow coefficients less than 0.267 (the point at which zero axial velocities at the hub and the "dip" in the overall performance characteristic curve are first noted), the two efficiency trends deviate sharply. At these operating conditions, blade-element efficiencies significantly larger than 100 percent were calculated in the hub region and begin to affect the mass-averaged values measurably even though the through-flow velocity in these regions is very low. Consequently, at flow coefficients below 0.267, the overall efficiency values represent values calculated from torquemeter measurements.

It is noted, also, that over the range of tip speeds covered herein and in reference 1 (representing a variation in blade chord Reynolds number from 1.09×10^6 to 2.18×10^6) there is no observable variation in overall efficiency with speed.

Blade-element data. - The value of individual blade-element performance both in analysis and as necessary background information of a design system has been established by the axial-flow compressor work. A similar approach to axial-flow-pump problems is made by presenting selected blade-element parameters in the following manner:

(1) Radial distributions at various flow coefficients. This presents an overall picture of the rotor and stage operation at various modes of operation. In this form operation at the higher blade tip speed

was selected for presentation. If similar curves at the lower speed are desired, they could be obtained using table I and the curves of element performance plotted.

(2) As a function of incidence angle. This provides necessary information for analysis and design of individual blade elements. In order to establish rotor-outlet velocity diagrams, relative outlet flow angle (from blade-outlet angle and deviation angle), the outlet tangential velocity (from ideal head coefficient), and blade speed may be used.

In general, the curves are self-explanatory; consequently, only more significant features will be pointed out. Figures 7, 8, and 9 present the radial distributions of the blade-element parameters and certain flow variables at the rotor inlet, rotor exit, and stator exit for $\varphi = 0.328$, 0.282, 0.267, and 0.252. Design variations are included where applicable. In figure 8 and many of the following figures the arrows pointing to the data points indicate that these points are off the scale. In most cases these points fall in the region of flow reversal where their numerical value is of little significance because of the large measurement errors encountered in such a region.

Comparison with design rotor. - For comparison with design, the observed performance at $\varphi = 0.282$ is used. At the rotor inlet the design and observed distributions closely approximate each other except in the tip region where the effects of tip casing boundary layer and tip clearance cavitation are probably being felt. The β_1 distribution also justifies the design assumption of no inlet whirl ($V_{\theta,1} = 0$).

A comparison of the design and measured rotor-outlet conditions at design flow coefficient indicates that

(1) The observed head rise is nearly constant across the passage, slightly higher than design in the tip region, and slightly lower than design at all other radii, and

(2) The measured efficiencies are close to the design values in the hub region, but decrease rapidly from the mean to the tip.

The head rise coefficient and efficiency of a pump are dependent upon the energy addition to the fluid ψ_i and the losses incurred in the flow process. In blade-element flow the losses should primarily be a function of the blade loading. Figure 8 shows that from the hub to the mean radius both the measured ψ_i and $\bar{\omega}$ compare favorably with the design variations, and this is reflected in the comparisons of measured head rise coefficient and efficiency with design values. From the mean section to the tip both the ψ_i and $\bar{\omega}$ are above design values (especially in tip region) with the result that, although the head rise coefficient approaches the design value, it occurs at a decreased efficiency. The energy addition is, in turn, dependent on the amount of turning of the

fluid done by the blade and (for the case of no inlet whirl) the outlet axial velocity. A measure of the turning done by the blade element is given by the deviation angle from the equation

$$\Delta\beta' = \kappa_1 - \kappa_2 + i - \delta$$

The axial-velocity distribution, of course, results from fulfilling both continuity and radial equilibrium requirements.

Stator. - Since the rotor and stators are close together and have constant hub and tip radii, the stator-inlet conditions are considered to be the same as the rotor-outlet conditions. All these parameters except the stator incidence angle have been discussed with the rotor performance. The stator incidence is plotted in figure 8(b).

At the stator exit a redistribution of axial velocity toward the hub occurs such that it compares to nearly the design inlet distribution. The total head distribution is quite uniform, and the stators turned the flow within 2.5° of the design direction (axial). For this type of design, level of axial velocity, and blade speed, a deviation of 2.5° from the design deviation angle of the stators would result in very small errors in the incidence angles of a succeeding rotor, approximately $\pm 0.2^\circ$ at the tip, $\pm 0.4^\circ$ at the mean, and $\pm 0.9^\circ$ at the hub element.

The loss coefficients that represent stator wake losses only (open symbols) show a low level of loss across the stators and very little variation with radius. Blade diffusion factors at both the hub and tip elements are approximately 0.52. These blade wake losses probably represent a minimum loss that will occur across a stator blade at this level of loading or diffusion. The marked increase in loss coefficient when the ideal total head is assumed to be the stator-inlet pressure (solid symbols) is difficult to explain. Additional free-stream losses (turbulent mixing of fluid leaving the rotor), secondary flow losses, circumferential pressure gradients at the two measuring stations, and errors in measurements all appear to be possible sources for the apparent increase, but, at present, it was not possible to isolate any individual effects.

Off-design performance. - The preceding discussion considered the distributions presented in figures 7 to 9 at the design φ. Next, the off-design distributions shown in figures 7 to 9 will be considered briefly. At the rotor inlet, the radial distributions of flow parameters were similar to the design distributions with the change of flow coefficient being reflected in the level of axial velocity. At the rotor outlet the rotor energy addition, by the nature of this type of rotor design, changes considerably at the tip but very little at the hub. Figure 10 illustrates the reason for this by graphically showing the effect of a change of axial velocity on typical velocity diagrams at tip and hub elements for this type of design. The diagrams of figure 10 also show that

the same reasoning applies to a change in turning angle (deviation angle), thus demonstrating the relative effects of small errors in axial velocity or deviation angle at the two radial stations.

To satisfy the requirements of radial equilibrium the axial-velocity distribution must shift with each change of flow coefficient. At higher than design φ the rotor-exit axial velocity is highest at the hub, while at lower than design φ the opposite trend is observed. If operation is continued to low enough φ, the axial-velocity gradient becomes so steep that axial velocities of zero are measured in the hub region, resulting in no flow or even reversed flow in this region. This type of operation first occurred in the rotor at a flow coefficient between 0.252 and 0.267. This is the same flow coefficient at which the "dip region" noted on the overall performance curve (fig. 6) occurs.

The energy addition and loss combine to give the distribution of head rise and efficiency shown in figure 8. It was found that in the region of zero axial velocities it was very difficult to obtain consistent measurements, particularly static heads, and this difficulty is reflected in the scatter of performance parameters based on static head in this region. The general decrease in the level of ϖ as φ is decreased (incidence increased) indicates that at design flow the blade elements were not operating at the minimum-loss incidence angles. The minimum-loss incidence angles will be discussed further in a later section.

In general, the radial distributions of blade-element and flow parameters at the stator exit reflect the changes induced by the rotor. At the lowest flow coefficient (φ = 0.252) the axial velocity also goes to zero in the hub region.

Blade-element data as a function of incidence angle: rotor. - For design and analysis of individual blade elements the element performance parameters are presented as functions of incidence angle. Such plots for both the rotor and stators are presented in figures 11 and 12, respectively, for blade elements situated at passage heights of 10, 30, 50, 70, and 90 percent from the tip. In the selection of blade elements representative of blade tip and hub, radii 10 percent of passage height from the inner and outer shrouds were chosen. At these locations, the effects of the casing boundary layers should be small, and the performance presented is considered to be influenced only by the flow conditions occurring around the blade element. To obtain representative overall performance values, some correction for the effects of the casing boundary layers must then be applied to such parameters as flow, head rise, and efficiency.

The data presented in figures 11 and 12 are the same noncavitating data presented in the preceding section plus data taken at a U_t of 123 feet per second. Again the curves are, in general, self-explanatory, and only significant observations will be discussed.

The design objective is to obtain the desired turning of the fluid with a minimum loss. Of primary interest to the designer would be the loss coefficient, deviation angle, and minimum-loss incidence angle. To aid in the analysis of the blade section, the blade-element parameters k, η, D, and ψ_i are included as functions of incidence angle.

In the tip region (fig. 11(a)) the data obtained were not sufficient to completely define a minimum-loss incidence angle. However, they do show that at an incidence angle of 3° to 4° the losses are significantly lower than at the design angle of incidence of approximately 1°. At the lowest loss point for a D factor of 0.32, a blade-element efficiency of 89 percent was measured. From this it would appear that the design incidence angle setting was primarily responsible for the low efficiencies obtained in the tip region at design φ. It is also interesting to note that the noncavitating performance at this radius was obtained at a k value of approximately 0.22.

The blade-element performance parameter obtained at a 30 percent passage height from the tip (fig. 11(b)) showed similar distributions with incidence angle to those observed at a 10 percent passage height (fig. 11(a)). While the minimum-loss incidence angle range was again not well-defined, the losses exhibited a rather sharp decrease as incidence angle was varied from the design value of approximately 1° to the lowest loss incidence angle of 4°. At the latter point an element efficiency of over 90 percent was attained.

At 50 and 70 percent passage height the variation of minimum-loss incidence angle is more representative of a typical characteristic $\bar{\omega}$ against i_r curve for a blade element. The minimum loss falls beneath the assumed design value and occurs at slightly higher incidence angles. At both stations efficiencies over 90 percent were attained.

At the hub element, 90 percent passage height, the $\bar{\omega}_r$ against i_r curve showed no minimum value. At φ's (incidence angles) where other elements showed lowest loss, measurements in the hub region show zero axial velocities and probable existence of eddy, or reverse flow, regions. Under these conditions the measurements, especially static pressure, are uncertain, and no attempt was made to place any meaning on the calculated element parameters utilizing static-pressure measurements. However, even at the loss level measured at the higher flow coefficients (low incidence angle), efficiencies from 87 to 90 percent are obtained. At an incidence angle of 4°, a D factor of approximately 0.67 was attained at an efficiency of 90 percent. This indicates that it may be possible to utilize blade loadings higher than the limit (D = 0.60) used in this design while maintaining good efficiency.

Blade element data as a function of incidence angle: stator. - Stator-blade-element parameters as a function of incidence angle are presented in figure 12. Since only the loss coefficients representing wake losses showed consistent trends, these alone are presented. Again the

minimum-loss incidence angles were not always completely defined, but approximate values can be obtained. For the type of stators used herein the minimum-loss incidence angles lie in the range of 0° to -5° at all radii. As mentioned earlier, the level of loss shown probably represents the minimum value that could be attained by this type of blade at this level of loading. (Because this type of loss coefficient could not be computed at all radii for all operating conditions, the number of points presented at each blade-element radial position will vary.)

In summary, the blade-element performance curves indicate that at design flow all rotor elements except the hub were not operating at a minimum-loss value. This accounts for the low efficiencies measured in the tip region at design φ. An attempt was made to predict the approximate potential capability of this type of rotor by applying the lowest measured loss coefficients at each element to the measured energy addition at design φ. Figure 13 shows the radial distribution of $\bar{\omega}$, ψ, and η that results and compares it to the design distributions. It is apparent from figure 13 that this performance would have met or even exceeded the overall design values.

Comparison with compressor data. - One of the expressed purposes of this design was to determine if the mass of information correlated from axial-flow-compressor data could be utilized in axial-flow pump design. Therefore, a comparison among the primary design parameters of loss coefficient and minimum-loss incidence and deviation angles as measured and computed from the design rules of reference 2 is presented. In figure 14 the pump blade section loss coefficients at the minimum-loss incidence angle are shown superimposed on the rotor and stator $\bar{\omega} \cos \beta'/2\sigma$ against D factor curves taken from reference 2. The results of this investigation indicate that the rotor losses follow the trend of axial-flow compressor losses and are lower in magnitude, especially in the rotor tip region. Although the experimental results of one specific pump do not justify any generalizations, the correlation does indicate the possibility of using compressor data with slight modifications to compute losses in pumps.

The blade-element performance curves and figure 10 have clearly shown the need for accurate values of design incidence and deviation angles. Incidence and deviation angles applied in the design of the rotor reported herein were computed from the design rules of reference 2. It was noted in axial-flow compressor results that reference incidence and deviation angles obtained in the three-dimensional environment of a rotor differed from those measured for the same blade shape when tested with the essentially two-dimensional flow through a cascade. As applied to design, reference 2 acknowledges these differences as a correction factor to the calculated values from empirical design rules based on the cascade tests ($i_{2\text{-}D}$ and $\delta_{2\text{-}D}$). Table II compares these correction factors ($i_c - i_{2\text{-}D}$ and $\delta_c - \delta_{2\text{-}D}$) advocated in reference 2 for low Mach number with those necessary to obtain the measured values at the minimum-loss (reference incidence angle) point ($i_p - i_{2\text{-}D}$ and $\delta_p - \delta_{2\text{-}D}$).

It is obvious from table II that the correction factors for reference incidence angle necessary to correlate the two-dimensional cascade results with the results obtained in a three-dimensional compressor environment are not applicable in this case. It should be recalled, however, that the majority of data used in reference 2 to obtain these empirical corrections was obtained from high Mach number rotor tests, and the low Mach number corrections are largely extrapolations of these data. However, until more data from pumps are available, no generalizations can be made.

A comparison of the measured deviation angles at reference incidence angle with those predicted by the equations of reference 2 indicated a varying degree of agreement at different blade sections. Again, more data are necessary before a general comparison can be attempted.

Cavitation Performance

As a pump is operated at successively lower net positive suction heads, or more fundamentally, lower blade cavitation numbers for each constant flow coefficient (similar inlet flow geometry), a characteristic curve is obtained which typically passes in a continuous manner through several regions of interest:

(1) Noncavitating region. Typical operation in this regime has been discussed in the preceding section and represents the performance of a pressure-type stage mentioned previously. As H_{SV} is lowered, this level of performance would be maintained until affected by cavitation. The initial effects of cavitation on performance signal the beginning of the second region.

(2) Cavitation inception region. Under these operating conditions, cavitation has a detrimental effect on the pump performance as compared to the noncavitating values. This area is generally defined as a region where a slight decrease in H_{SV} or k results in a small dropoff in performance. For operation in water this region is generally a narrow one, and the final region of operation is quickly reached.

(3) Cavitation breakdown region. Cavitation breakdown occurs when a slight decrease in H_{SV} or k results in a large decrease in performance. Severe cavitation is encountered in this region.

For investigations where this type of performance curve is well defined, cavitation inception and breakdown may be located as points on the curve. The cavitating performance presented herein does not contain sufficient data to identify these points, but does serve to demonstrate operation near these distinct points.

Overall Performance

Figure 15 presents the overall performance in terms of flow coefficient, head rise coefficient, and efficiency for a blade tip speed of 123 feet per second and net positive suction heads of 115, 45, and 33 feet. These three inlet heads correspond to suction specific speeds at design φ of approximately 6,000, 13,000, and 16,000, respectively. The head-flow characteristic curve for H_{SV} = 115 feet is the same noncavitating performance curve shown in figure 6 and is repeated for comparative purposes. The overall performance curve for H_{SV} = 45 feet represents the type of curve expected when small amounts of cavitation (cavitation inception region) occur as associated with the inlet-type stage noted earlier. The remaining performance curve at H_{SV} = 33 feet represents operation under severe cavitating conditions (cavitation breakdown). One feature of figure 15 is the manner in which the H_{SV} = 115 feet and H_{SV} = 45 feet curves converge at φ = 0.267 and diverge slightly at flow coefficients above and below this value. This point of convergence occurs at the maximum efficiency point of each operating curve.

Blade-Element Data

Design point. - To compare the radial variation of blade-element parameters, performance at maximum efficiency (φ = 0.267) was selected (figs. 16, 17, and 18), since this is the probable region of design interest. Although the H_{SV} = 33 feet performance did not extend to this flow coefficient, operation at the highest φ = 0.255 was included for comparison.

A comparison of the radial distributions of rotor performance at H_{SV} = 45 feet indicates little fall-off in performance of the rotor for a large change in k. The difference in overall performance noted in figure 15 is due primarily to a dropoff in tip region performance. At all other radii the performance was very comparable. The axial-velocity distributions indicate slight flow shifts toward the hub. The cavitation number k at the tip element for this operating condition is 0.12. Cavitation has evidently affected the tip region performance but apparently has not yet affected the performance at the other radii. Thus this value may serve as a guide to the lower limits of k at which a blade of this type, level, and distribution of blade loading, and thickness will operate before its performance is severely impaired because of cavitation. As the design value of k for an inlet type stage is decreased, the head rise requirements of the inducer are lowered.

Changing H_{SV} from 45 to 33 feet indicates a large fall-off in rotor performance for a small change in k. At H_{SV} = 33 feet the effects of cavitation are being felt at all radii and are reflected in the higher losses and larger deviation angles measured at all radii and the resulting decreased performance as noted. The axial-velocity distribution

behind the rotor shows increased flow shifts toward the hub region. The tip element k value is 0.09, pointing up the small change in k to go from cavitation inception to cavitation breakdown when operating in water.

Stator-outlet flow conditions largely reflect the effects of cavitation on rotor performance. Mass-flow shifts toward the hub and the increased dropoff in head rise in the mean and tip regions noted for the cavitating rotor performance are also observed at the stator exit. Rotor cavitation appears to have little effect on stator loss - either wake loss or overall stator loss - at this operating condition. Stator deviation angles are slightly lower in the blade mean-radius area than those measured at higher net positive suction head operation.

Blade-element data as a function of incidence angle. - The rotor-blade-element data plotted as a function of incidence angle in figure 19 present the cavitating performance over the whole range of operation. As the mode of operation is changed from an H_{SV} of 115 to 45 feet, a change in performance is noticeable primarily in the tip measuring station. Both losses and deviation angles increase at this station. At all other radial stations minimum-loss incidence angles, loss level, and deviation angles are generally the same as measured for the noncavitating flow. Apparently, at all operating conditions blade cavitation is sufficient to measurably affect only the tip element of this rotor.

At the H_{SV} = 33 feet mode of operation the blade-element performance parameters do not show a consistent trend with incidence angle. The comparatively narrow flow range, covering a variation of incidence angle of slightly over 1°, places stringent requirements on measurements of flow. Also, the ability to set and maintain inlet flow conditions for the time needed to complete the passage surveys becomes increasingly important at these low inlet pressures. Although a trend with incidence angle is not clear, the curves do show some of the effects of cavitation on the blade-element performance. In general, as cavitation is intensified (H_{SV} lowered), the losses and deviation angle are increased, and the head rise coefficient and efficiency may be expected to decrease. At H_{SV} = 33 feet for this rotor, these effects are most pronounced in the tip region and decrease with radius.

The stator-blade-element performance parameters are plotted as functions of incidence angle in figure 20. As before, only the blade wake loss coefficients are presented. Although the number of wake loss coefficients that could be computed at the H_{SV} = 33 feet mode of operation was limited, those available do not show any significant change in either the loss level or location of minimum-loss incidence angles from the noncavitating results. Deviation angle calculations also indicate that cavitation in the rotor, at least to the degree obtained in this investigation, had a negligible effect on stator deviation angle.

Validity of Simple Radial Equilibrium Assumption

In the design of the rotor used in this investigation, simple radial equilibrium (neglecting effects of radial motion) was assumed behind the rotor to define the flow conditions. The validity of this assumption can be estimated by utilizing the measured flow angles and total head distribution in the modified simple radial equilibrium equation to calculate axial-velocity distributions. The calculation procedure consisted of assuming tip axial velocities in an iterative process until flow continuity was achieved. A comparison of calculated axial-velocity distributions by simple radial equilibrium with the experimentally measured axial-velocity distributions is presented in figures 21 and 22 for the following conditions:

U_t	H_{sv}	φ
154	115	0.328
		.282
		.267
		.252
123	33	0.255
		.240
		.224

These comparisons indicate that the simple radial equilibrium expression adequately describes the radial-velocity gradient at all modes of operation, both noncavitating and cavitating. In this demonstration the calculations utilized measured values of total head and angle, which means that exact distribution of axial velocity to variations of the loss and deviation angle may be obtained from reference 6, which computes the effects of systematically varying each parameter.

SUMMARY OF RESULTS

An analysis of the blade-element data obtained from an investigation of an axial-flow pump designed by blade-element theory indicated:

1. At design flow coefficient, greater than design energy input was achieved, particularly at the rotor tip. The efficiency, however, was lower than anticipated and the resulting total head rise was slightly lower than the design value.

2. The anticipated efficiencies were not achieved at design flow coefficient because all blade elements except the hub were not operating at the minimum-loss (reference) incidence angles.

3. A comparison of the performance results of this rotor with values anticipated by the design equations of NACA RM E56B03a indicated that:

(a) At reference incidence angle, the losses at all radii were less than those indicated in RM E56B03a.

(b) Some modification of the design equations of RM E56B03a is necessary for the accurate prediction of minimum-loss incidence and deviation angles of axial-flow pumps.

4. At the maximum overall efficiency the rotor performance began to drop off because of cavitation effects (cavitation inception region) at a cavitation number k of approximately 0.12 (suction specific speed $\approx$ 13,000). This initial fall-off resulted from a decrease in tip region performance.

5. Over a majority of the flow range the stators turned the fluid back to within a few degrees of the axial direction, indicating that this type of stage design could be perpetuated. A $\pm 2^{\circ}$ variation in outlet angle would have a very small effect (especially in the tip region) on the incidence angle of a succeeding rotor.

6. The simple radial equilibrium expression adequately describes the radial pressure gradient at all modes of operation, both noncavitating and cavitating.

Lewis Research Center
National Aeronautics and Space Administration
Cleveland, Ohio, September 8, 1961

APPENDIX A

SYMBOLS

c	blade chord, in.
D	blade diffusion factor, defined as $D = 1 - \frac{V_2'}{V_1'} + \frac{\Delta V_\theta'}{2\sigma V_1'}$ (see ref. 1)
g	acceleration due to gravity, 32.17 ft/sec^2
H	total head, ft
H_{sv}	net positive suction head, $H - h_v$, ft
h	static head, ft
h_v	vapor head, ft
i	incidence angle, deg
k	cavitation number, $(h_1 - h_v)/[(V_1')^2/2g]$
N	rotative speed, rpm
Q	flow rate, gal/min
r	radius, in.
SS	suction specific speed, $N\sqrt{Q}/(H_{sv})^{3/4}$
s	blade circumferential spacing, in.
U	rotor tangential velocity, ft/sec
V	absolute velocity, ft/sec
β	flow angle, angle between direction of flow and axial direction, deg
γ	blade setting angle, deg
δ	outlet deviation angle, deg
η	efficiency, percent
κ	angle between camber line and axial direction, deg
σ	blade solidity, c/s

φ flow coefficient, V_z/U_t

ψ ideal (no-loss) head rise, defined (for case of no inlet whirl) as

$$\psi_i = \frac{U_2 V_{\theta,2}}{U_t^2}$$

ψ_r rotor head rise coefficient, $\frac{g(H_2 - H_1)}{U_t^2}$

ψ_{ST} stage head rise coefficient, $\frac{g(H_3 - H_1)}{U_t^2}$

$\bar{\omega}$ relative total head loss coefficient

Subscripts:

c compressor

e error

i ideal

n radial position

p refers to data obtained from investigations of pump rotors

r rotor

ST stage

s stator

t tip

v measured with Venturi

z axial component

θ tangential component

1 measuring station at rotor inlet

2 measuring station at rotor exit (stator inlet)

2-D refers to values obtained from two-dimensional cascade data

3 measuring station at stator exit

Superscripts:

– mass averaged

' relative to rotor

* axial velocity calculated by simple radial equilibrium

APPENDIX B

EQUATIONS

Blade element:

Ideal head rise (assumes $V_{\theta,1} = 0$):

$$(H_2 - H_1)_i = \frac{UV_{2,\theta}}{g}$$

Rotor efficiency, percent:

$$\eta_r = \frac{100(H_2 - H_1)}{(H_2 - H_1)_i}$$

Stage efficiency, percent:

$$\eta_{ST} = \frac{100(H_3 - H_1)}{(H_2 - H_1)_i}$$

Rotor relative total head loss coefficient:

$$\bar{\omega}_r = \frac{H'_{2,i} - H'_2}{\frac{(V'_1)^2}{2g}} = \frac{\Delta H_{loss}}{\frac{(V'_1)^2}{2g}} = \frac{(H_2 - H_1)_i - (H_2 - H_1)}{\frac{(V'_1)^2}{2g}}$$

Stage total head loss coefficient:

$$\bar{\omega}_s = \frac{H_{3,i} - H_3}{\frac{V_2^2}{2g}}$$

Blade diffusion factor (assumes constant radius element):

$$D = 1 - \frac{V'_2}{V'_1} + \frac{\Delta V'_\theta}{2\sigma V'_1}$$

Cavitation number:

$$k = \frac{h_1 - h_v}{\frac{(V'_1)^2}{2g}}$$

Overall:

Integrated volume flow:

$$Q = 2\pi \frac{448.8}{144} \int V_z r \, dr$$

Percentage error between integrated and Venturi volume flows:

$$Q_e = 1 - \frac{Q}{Q_v}$$

Area-averaged axial velocity:

$$\overline{V}_z = \frac{\int V_z r \, dr}{\int r \, dr}$$

Mass-averaged total head:

$$\overline{H} = \frac{\int H V_z r \, dr}{\int V_z r \, dr}$$

Mass-averaged efficiency:

$$\overline{\eta} = \frac{\int \eta V_z r \, dr}{\int V_z r \, dr}$$

Radial equilibrium:

$$(V^*_{2,z})^2 = \frac{2g \left[(H_2)_n - (H_2)_{n+1}\right] (V_{2,z})^2_n \left[\tan^2(\beta_2)_n \left(2 - \frac{V_n + 1}{r_n}\right) + 1\right]}{\tan^2(\beta_2)_{n+1} \left(\frac{r_n}{r_{n+1}} - 2\right) - 1}$$

Simple radial equilibrium equation for calculating axial-velocity distribution from the distribution of total head and total angle. The principal assumption here is the distance from r_n to $n + 1$ station is close enough that $\frac{V_\theta^2}{gr} dr$ can be expressed as a linear variation.

REFERENCES

1. Crouse, James E., Montgomery, John C., and Soltis, Richard F.: Investigation of the Performance of an Axial-Flow-Pump Stage Designed by the Blade-Element Theory - Design and Overall Performance. NASA TN D-591, 1961.

2. Members of the Compressor and Turbine Research Division: Aerodynamic Design of Axial-Flow Compressors. Vol. II. NACA RM E56B03a, 1956.

3. Ross, C. C., and Banerian, Gordon: Some Aspects of High-Suction Specific-Speed Pump Inducers. Trans. ASME, vol. 78, no. 8, Nov. 1956, pp. 1715-1721.

4. Lieblein, Seymour, Schwenk, Francis C., and Broderick, Robert L.: Diffusion Factor for Estimating Losses and Limiting Blade Loadings in Axial-Flow-Compressor Blade Elements. NACA RM E53D01, 1953.

5. Hartmann, Melvin J., and Soltis, Richard F.: Observation of Cavitation in a Low Hub-Tip Ratio Axial Flow Pump. Paper 60-HYD-14, ASME, 1960.

6. Montgomery, John C.: Analytic Performance Characteristics and Outlet Flow Conditions of Constant and Variable Lead Inducers for Cryogenic Pumps. NASA TN D-583, 1961.

TABLE I. - BLADE DESIGN VALUES (CIRCULAR-ARC SECTIONS)

Radial position, percent passage height from tip	Blade section radius (inlet and outlet), in.	Blade-inlet angle, deg	Blade-outlet angle, deg	Blade solidity	Blade thickness-to-chord ratio
Rotor					
10	4.25	72.0	65.6	1.07	0.097
30	3.70	69.5	60.5	1.23	.091
50	3.15	66.4	52.4	1.44	.085
70	2.60	62.4	38.4	1.74	.079
90	2.05	53.4	10.0	2.21	.073
Stator					
10	4.25	33.1	-12.2	1.01	0.08
30	3.70	36.4	-11.6	1.16	.08
50	3.15	40.2	-11.2	1.36	.08
70	2.60	44.3	-10.9	1.65	.08
90	2.05	49.0	-10.6	2.09	.08

TABLE II. - COMPARISON OF MEASURED MINIMUM-LOSS INCIDENCE AND DEVIATION ANGLES WITH THOSE ANTICIPATED BY DESIGN RULES (REF. 2)

Percent passage from tip	$i_p - i_{2\text{-}D}$ (Noncavitating), deg	$i_c - i_{2\text{-}D}$ (M = 0), deg	$\delta_p - \delta_{2\text{-}D}$ (Noncavitating), deg	$\delta_c - \delta_{2\text{-}D}$ (M = 0), deg
Rotor				
10	3.4	-2.5	-1.4	-1.5
30	3.3	-2.0	-1.2	-1.0
50	2.5	-1.5	-.5	-.5
70	.8	-1.0	2.3	.1
90	1.8	-.5	3.2	1.0
Stator				
10	4.4	-2.5	2.2	-1.5
30	5.0	-2.0	-.6	-1.0
50	2.5	-1.5	-.7	-.5
70	-.5	-1.0	-1.9	.1
90	-3.7	-.5	-2.5	1.0

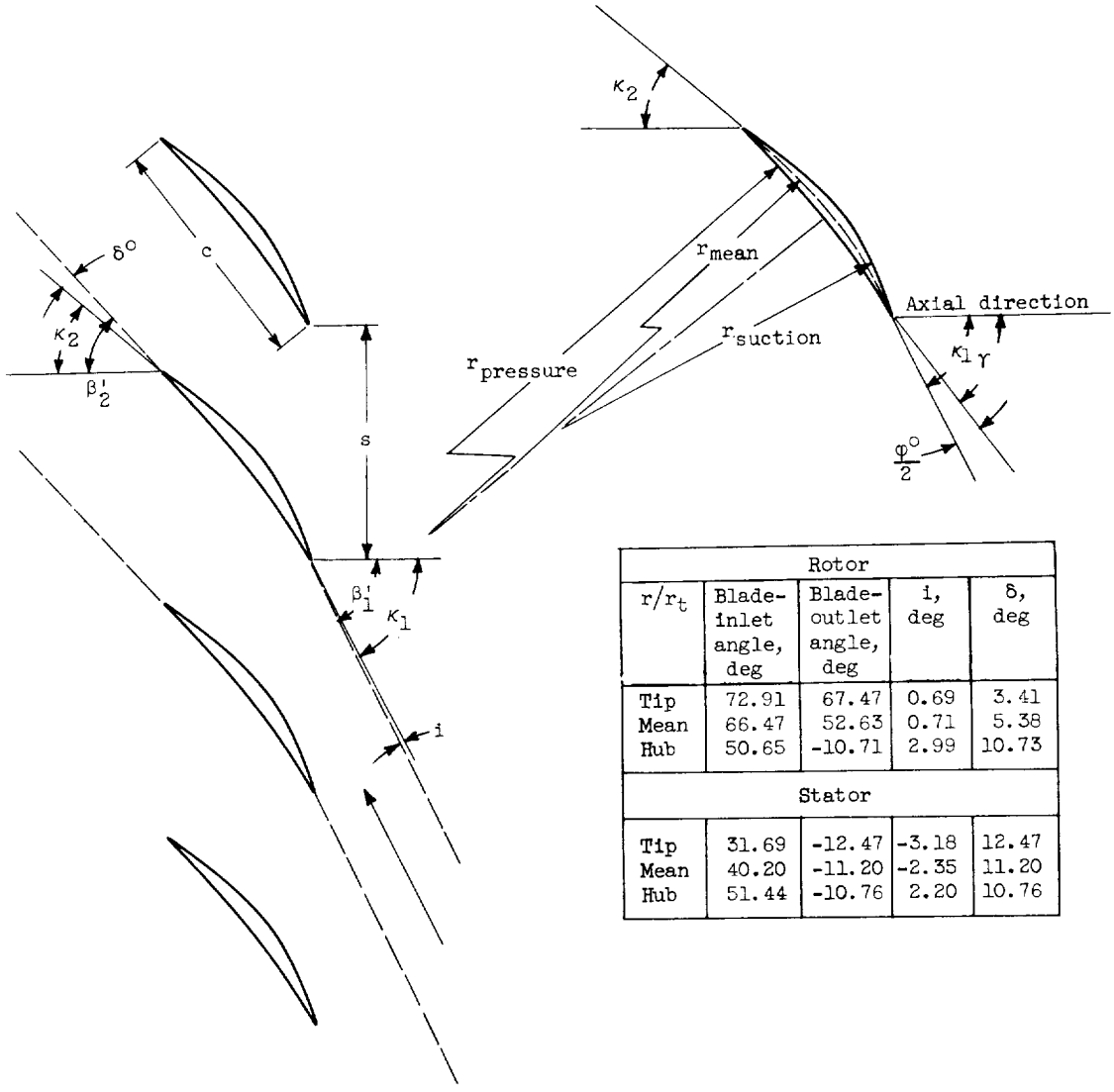

Rotor				
r/r_t	Blade-inlet angle, deg	Blade-outlet angle, deg	i, deg	δ, deg
Tip	72.91	67.47	0.69	3.41
Mean	66.47	52.63	0.71	5.38
Hub	50.65	-10.71	2.99	10.73
Stator				
Tip	31.69	-12.47	-3.18	12.47
Mean	40.20	-11.20	-2.35	11.20
Hub	51.44	-10.76	2.20	10.76

Figure 1. - Blade nomenclature.

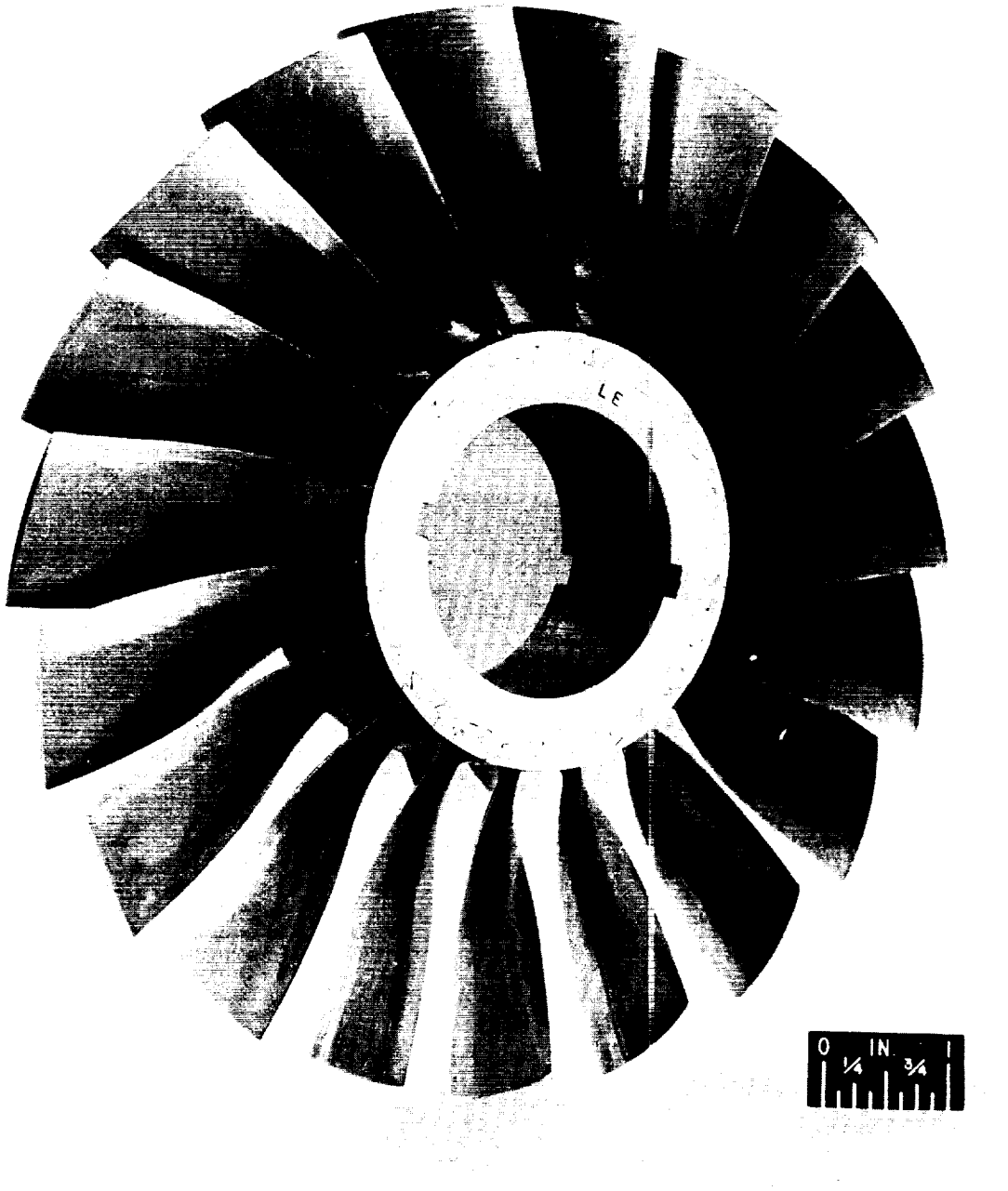

C-49981

Figure 2. - Axial-flow-pump rotor.

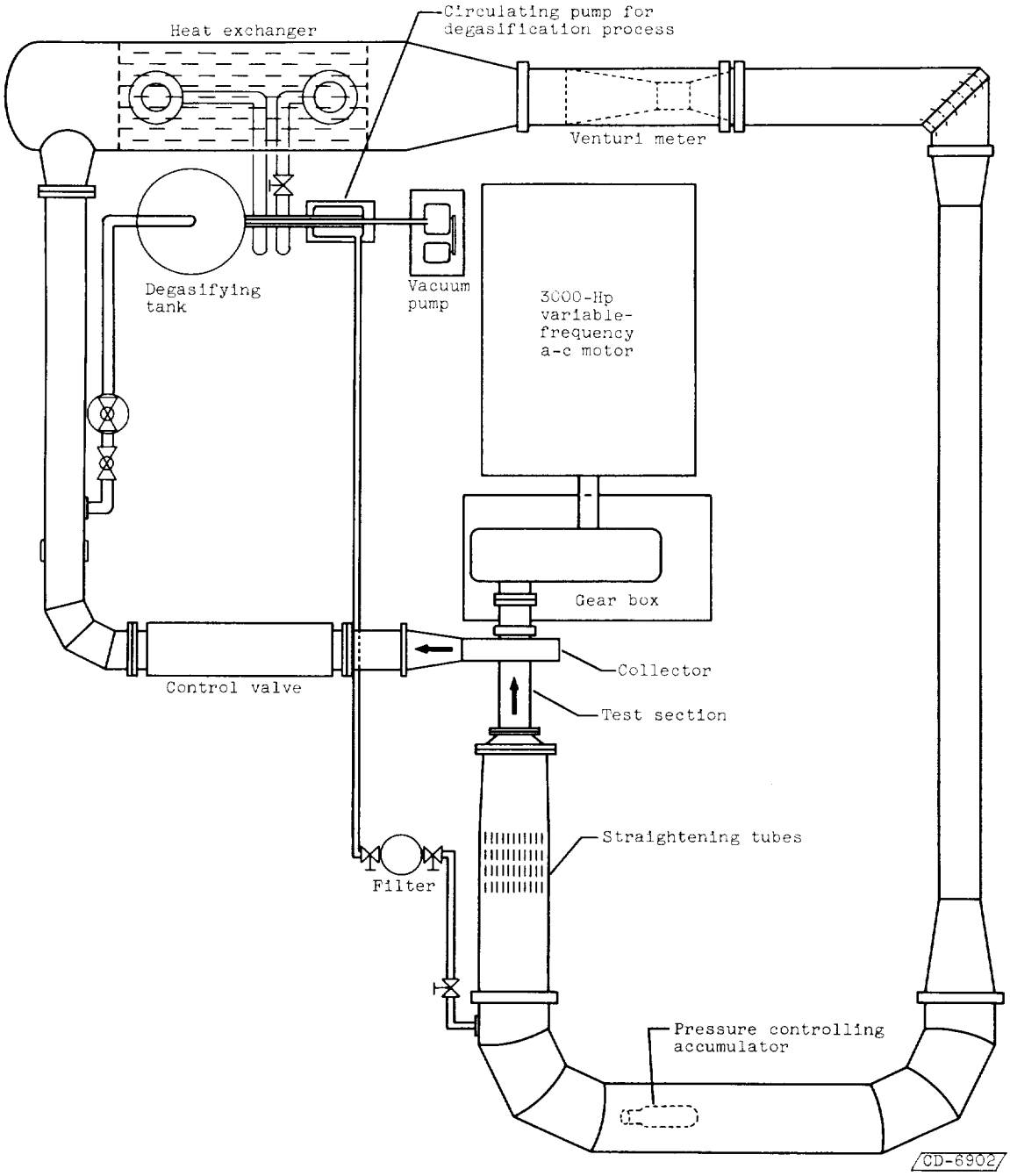

Figure 3. - Lewis water tunnel.

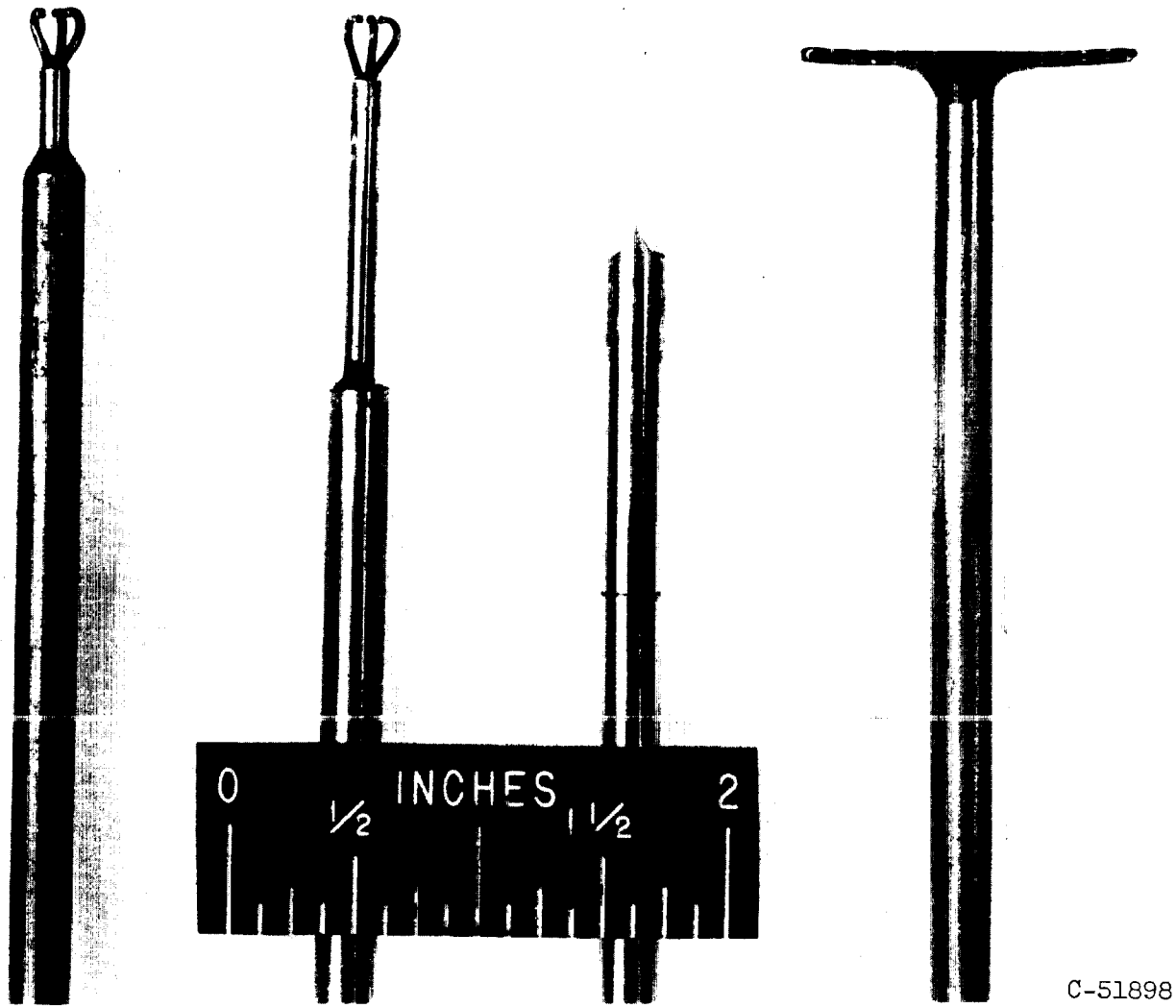

Total-pressure claws Static-pressure wedge Total-pressure rake

Figure 4. - Probes.

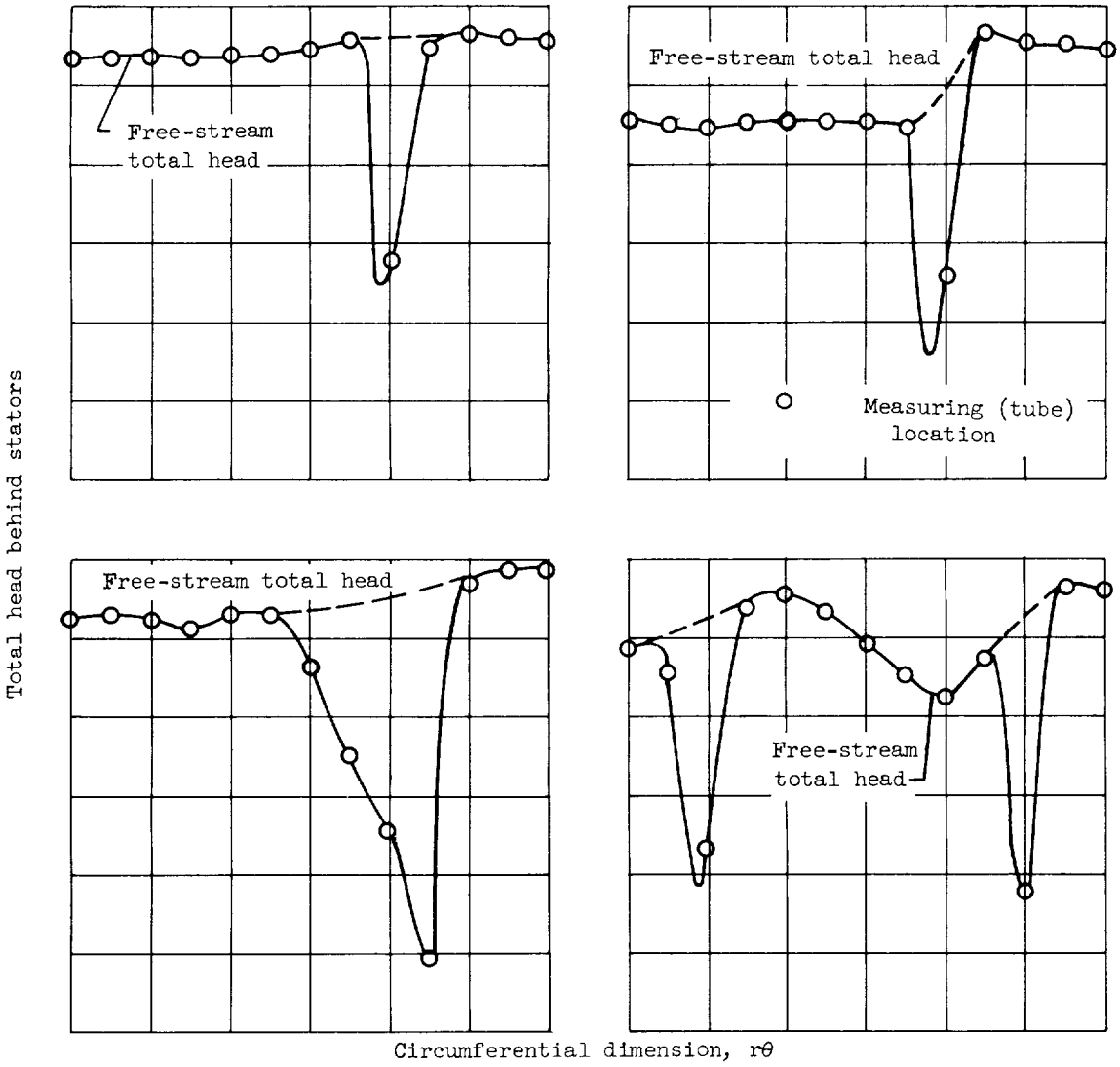

(a) Clearly defined wakes.

Figure 5. - Total head distributions behind stators.

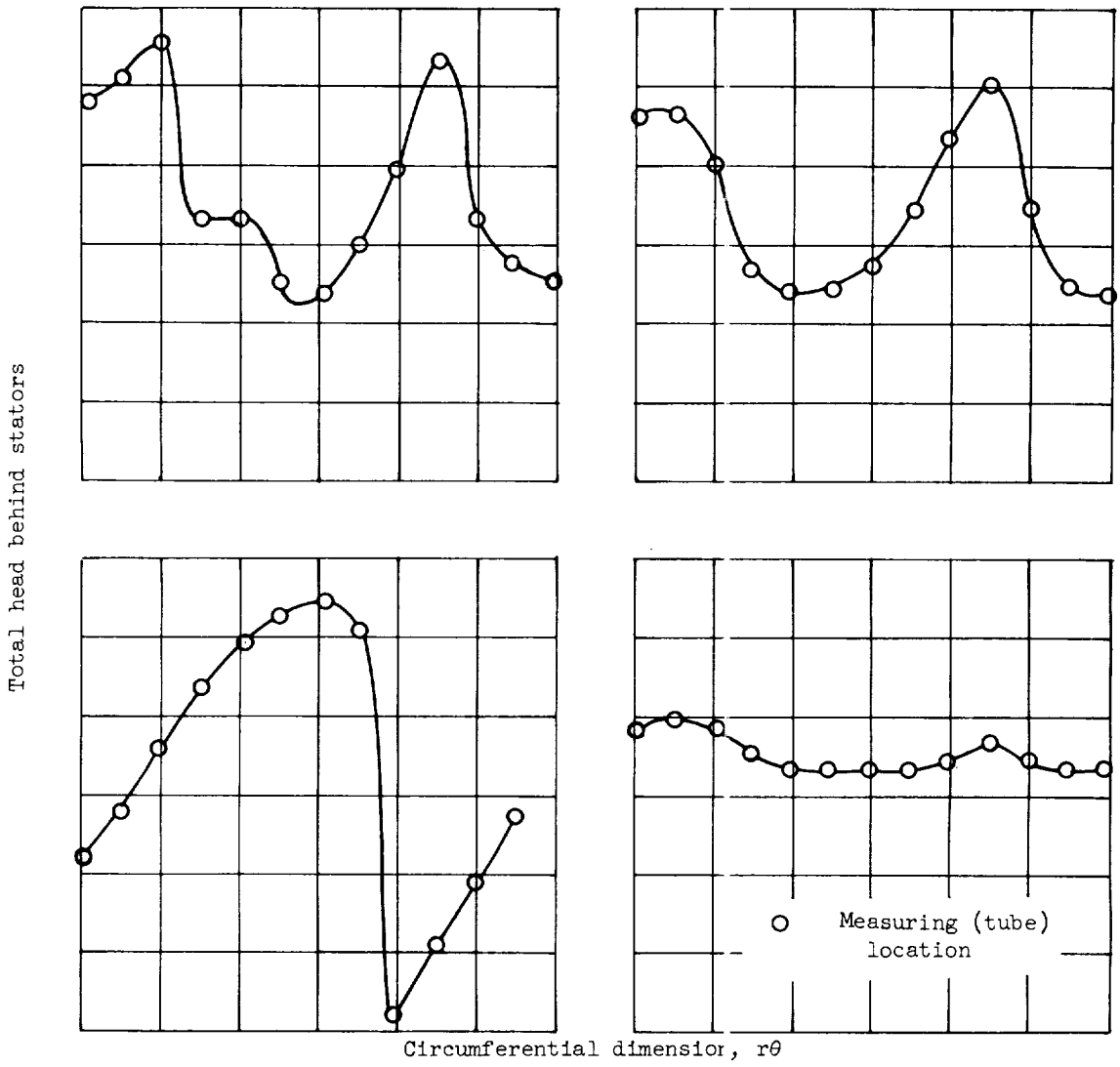

(b) Wakes not clearly discernible.

Figure 5. - Concluded. Total head distributions behind stators.

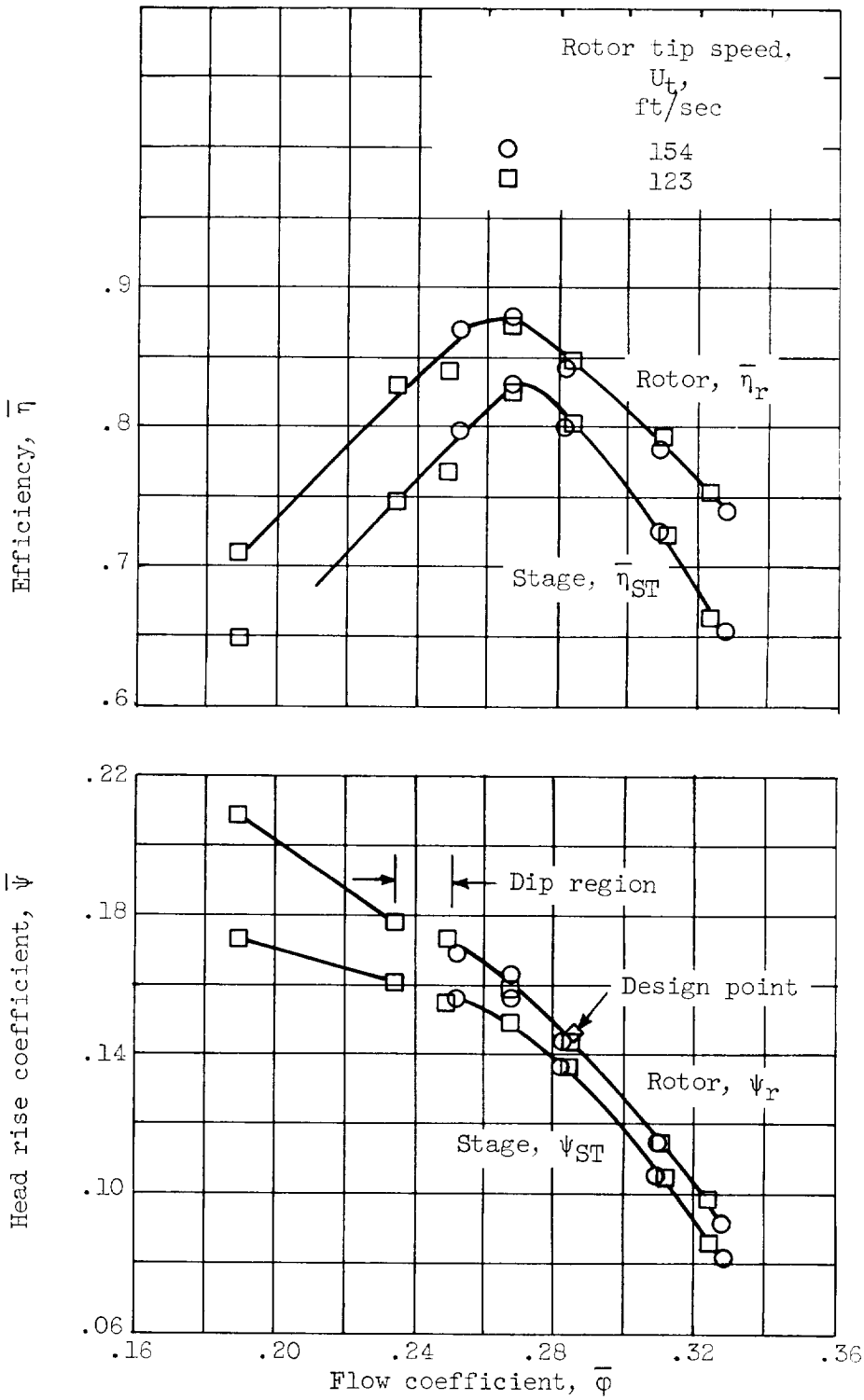

Figure 6. - Overall performance of axial-flow pump stage (noncavitating). Net positive suction head H_{sv}, 115 feet.

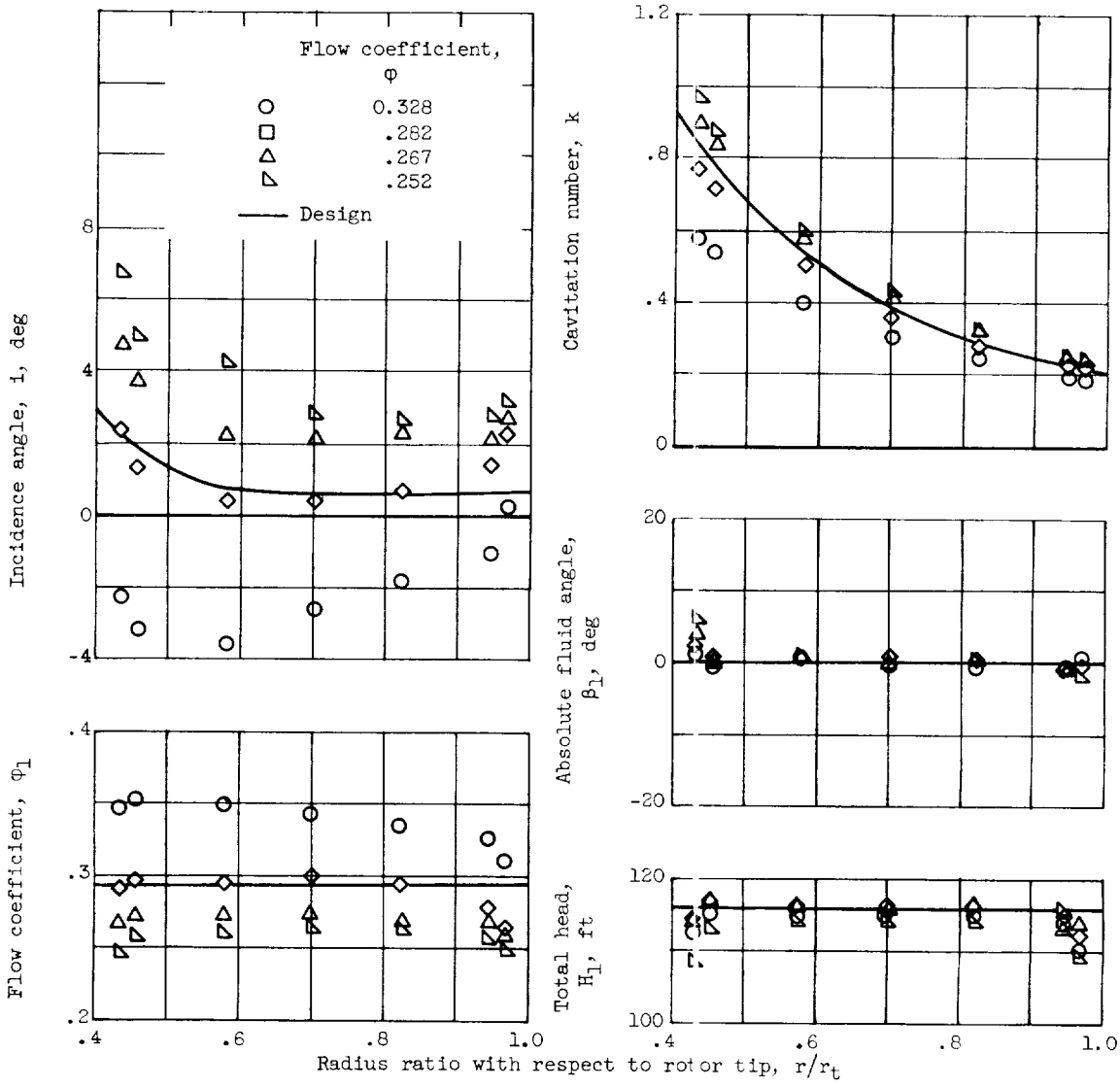

Figure 7. - Radial distribution of flow and blade-element performance parameters at rotor inlet (noncavitating). Rotor tip speed, 154 feet per second; suction head, 115 feet.

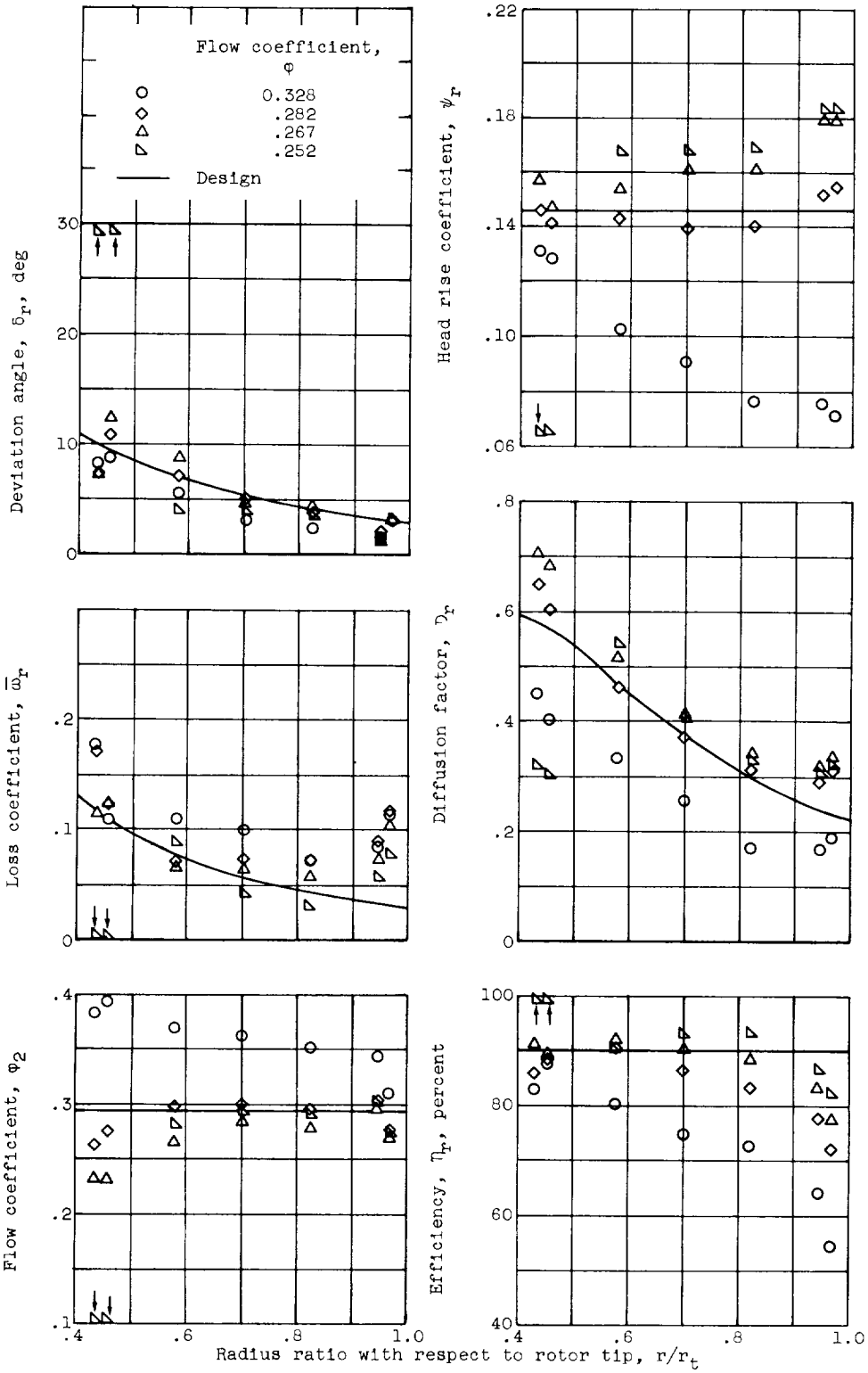

Figure 8. - Radial distribution of flow and blade-element parameters at rotor outlet (stator inlet) (noncavitating). Rotor tip speed, 154 feet per second; suction head, 115 feet.

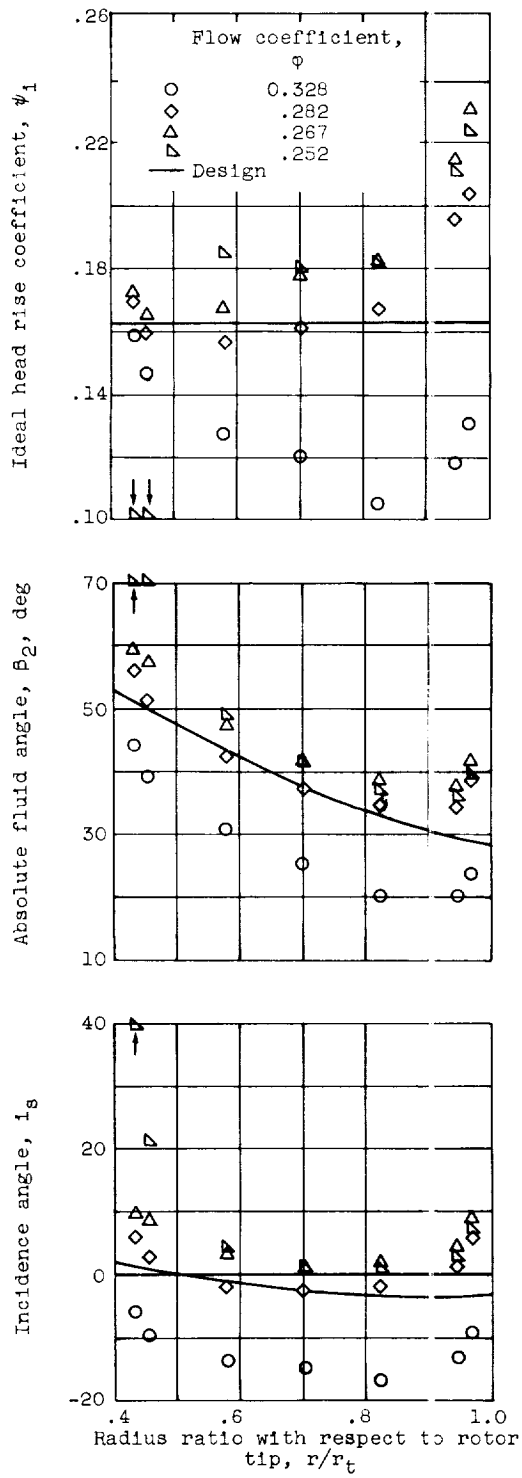

Figure 8. - Concluded. Radial distribution of flow and blade-element parameters at rotor outlet (stator inlet) (noncavitating). Rotor tip speed, 154 feet per second; suction head, 115 feet.

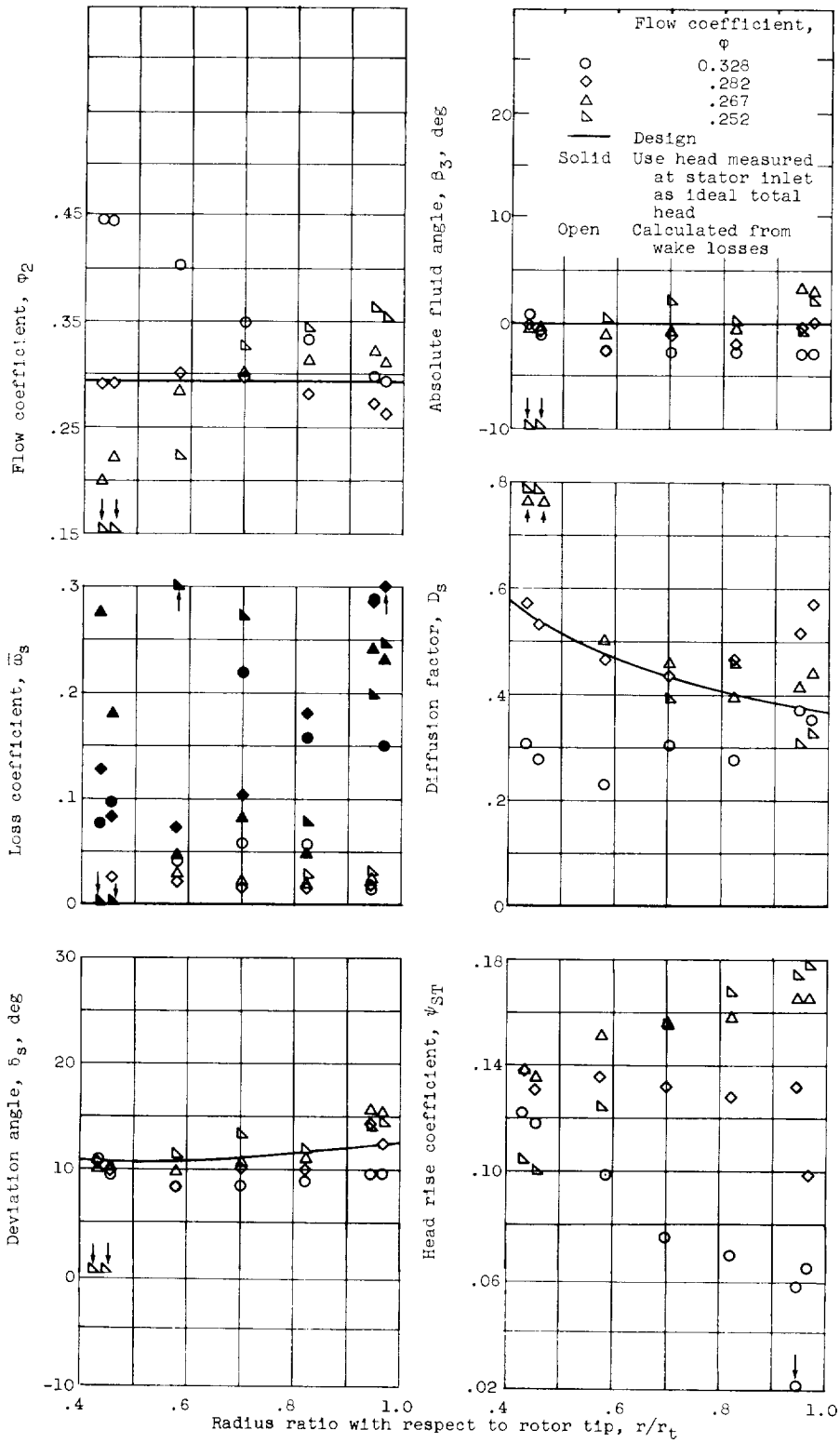

Figure 9. - Radial distribution of flow and blade-element parameters at stator outlet (noncavitating). Rotor tip speed, 154 feet per second; suction head, 115 feet.

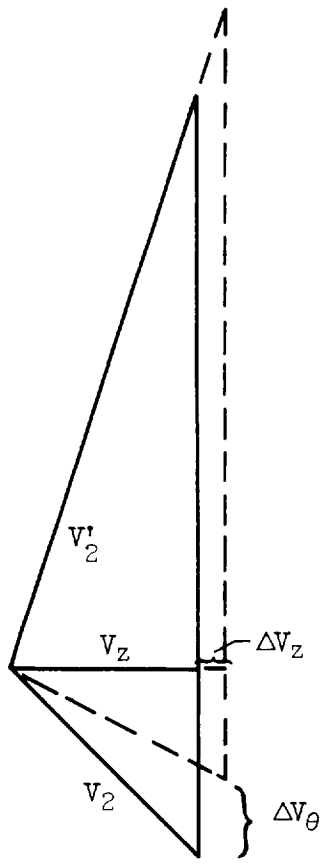

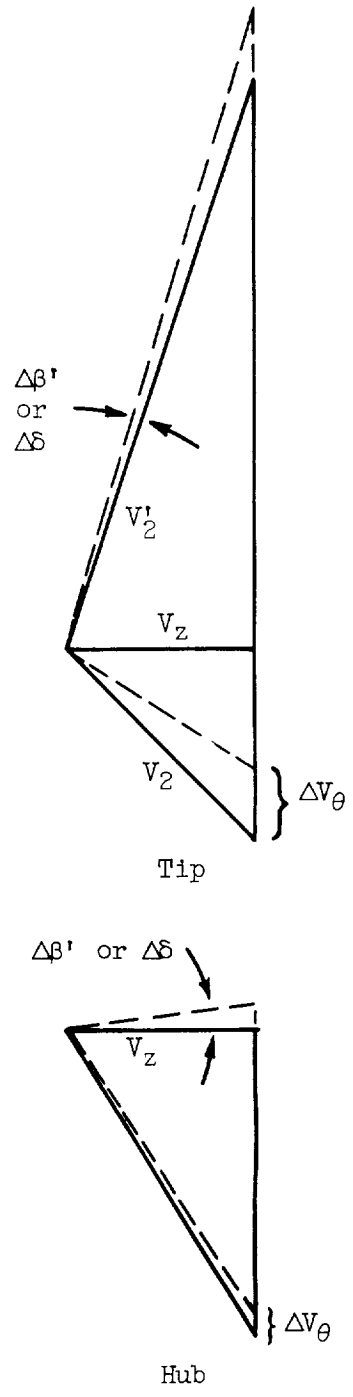

Change in axial velocity

Change in deviation angle

Figure 10. - Effect of variations of axial velocity and deviation angle on rotor energy addition.

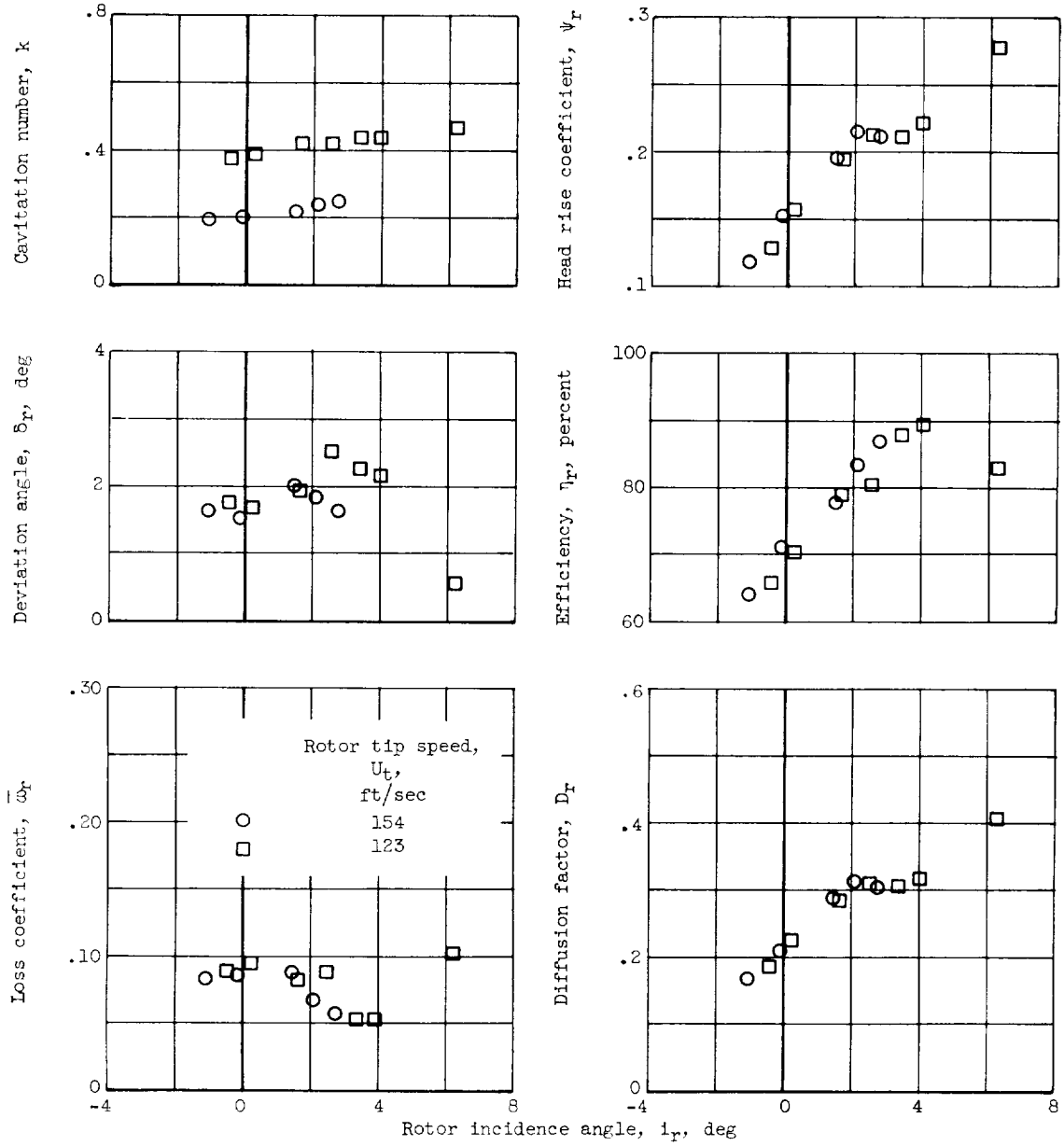

(a) 10 Percent passage height from tip.

Figure 11. - Rotor blade-element characteristics (noncavitating). Suction head, 115 feet.

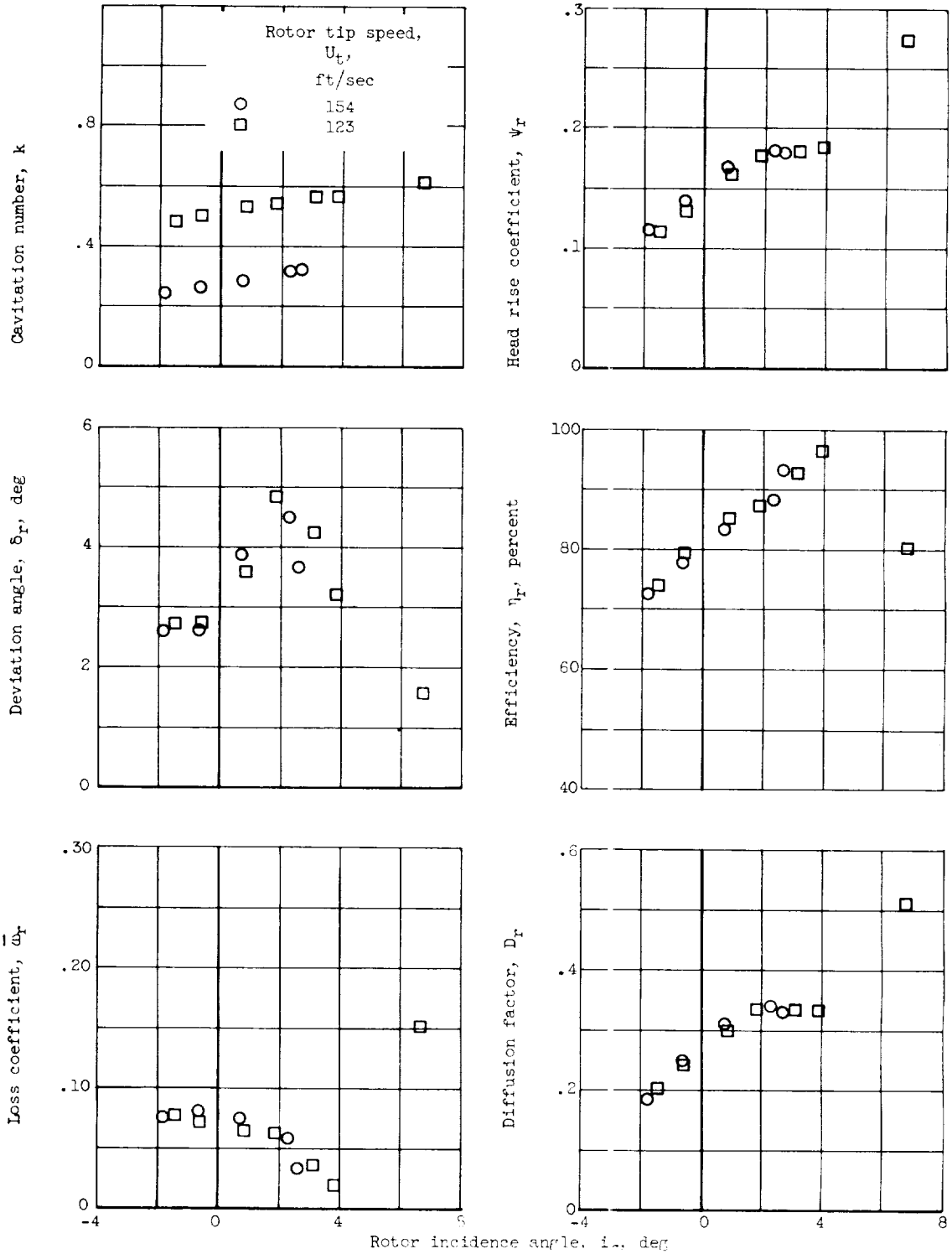

(b) 30 Percent passage height from tip.

Figure 11. - Continued. Rotor blade-element characteristics (noncavitating). Suction head, 115 feet.

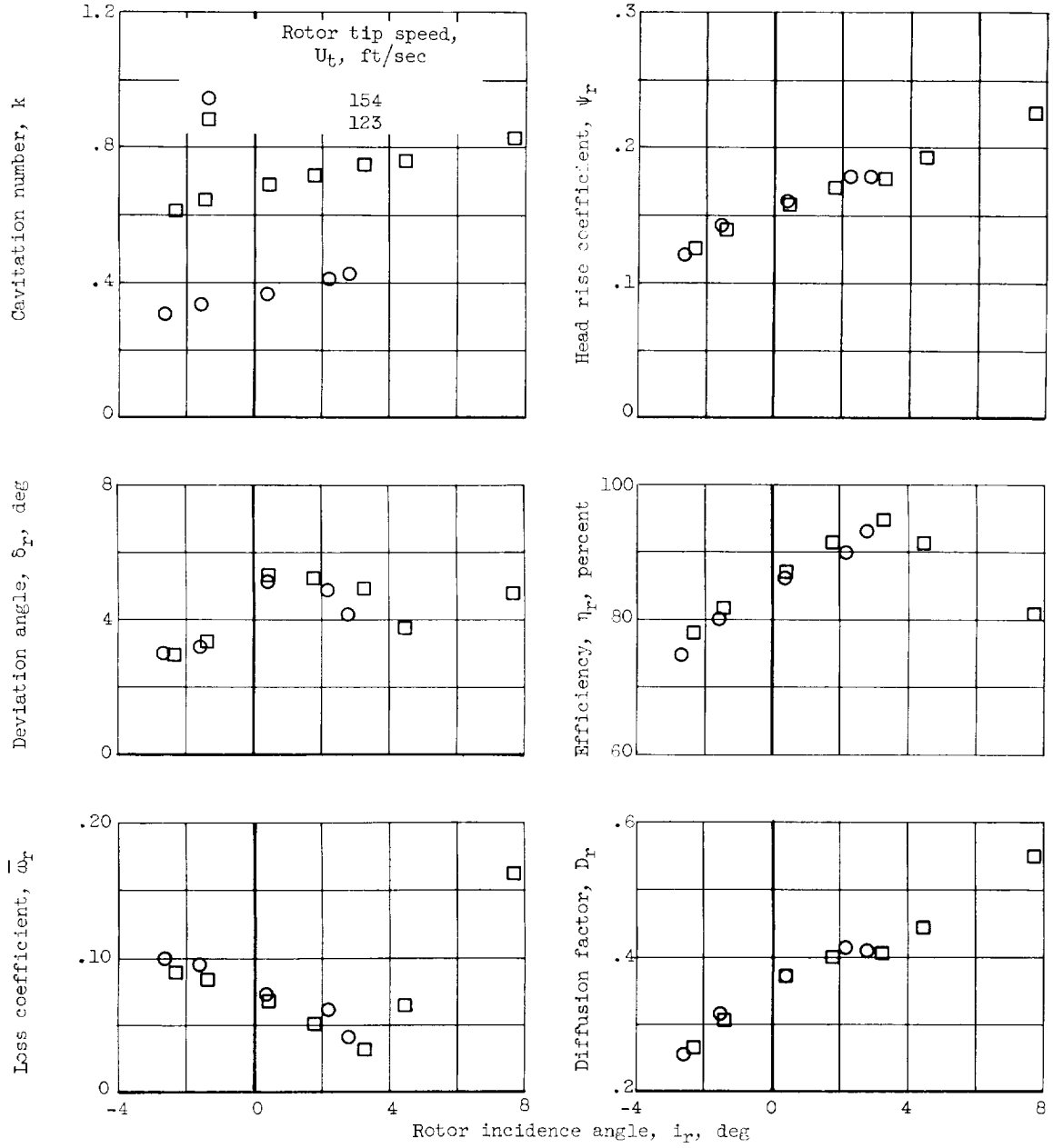

(c) 50 Percent passage height from tip.

Figure 11. - Continued. Rotor blade-element characteristics (noncavitating). Suction head, 115 feet.

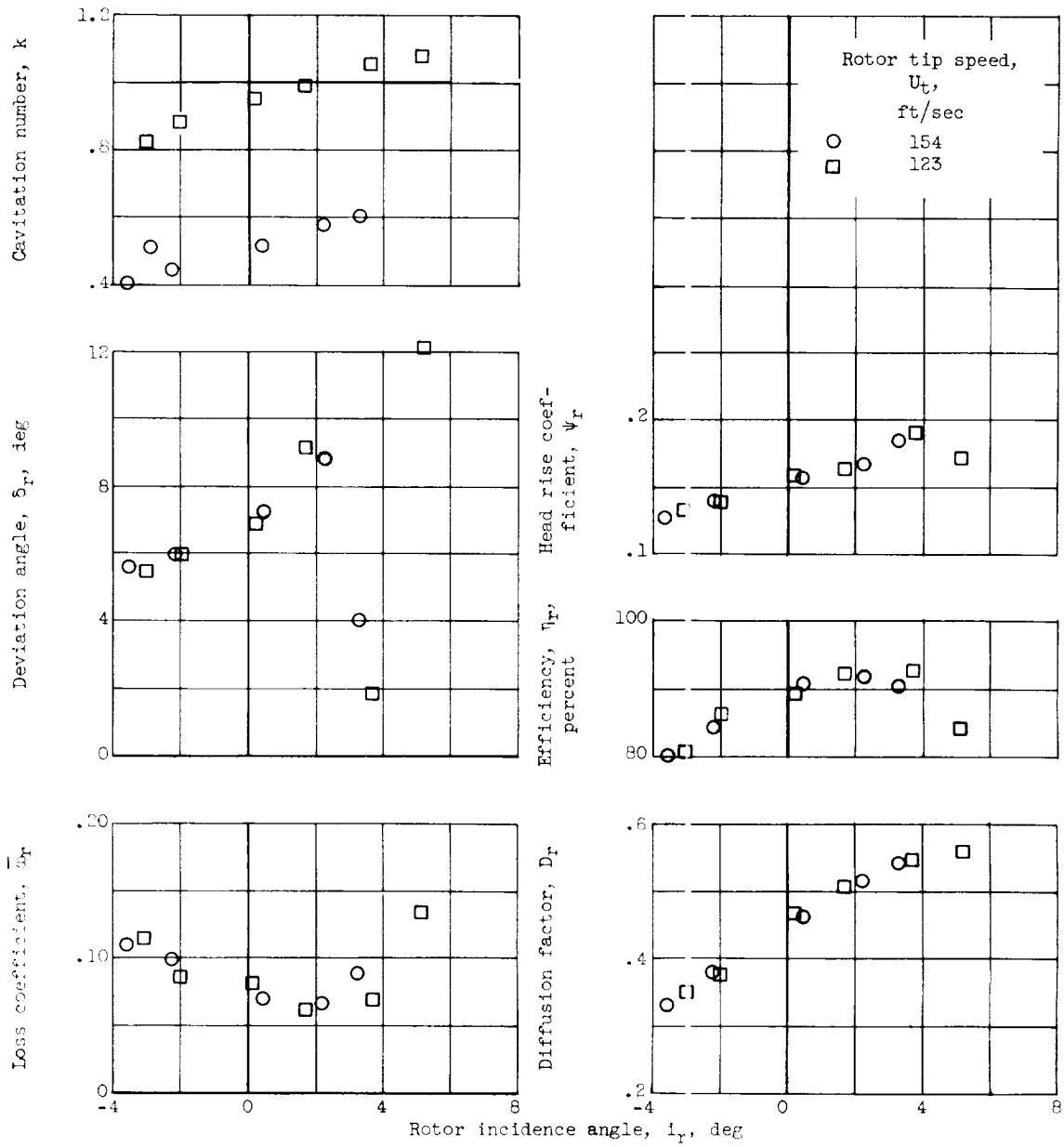

(d) 70 Percent passage height from tip.

Figure 11. - Continued. Rotor blade-element characteristics (noncavitating). Suction head, 115 feet.

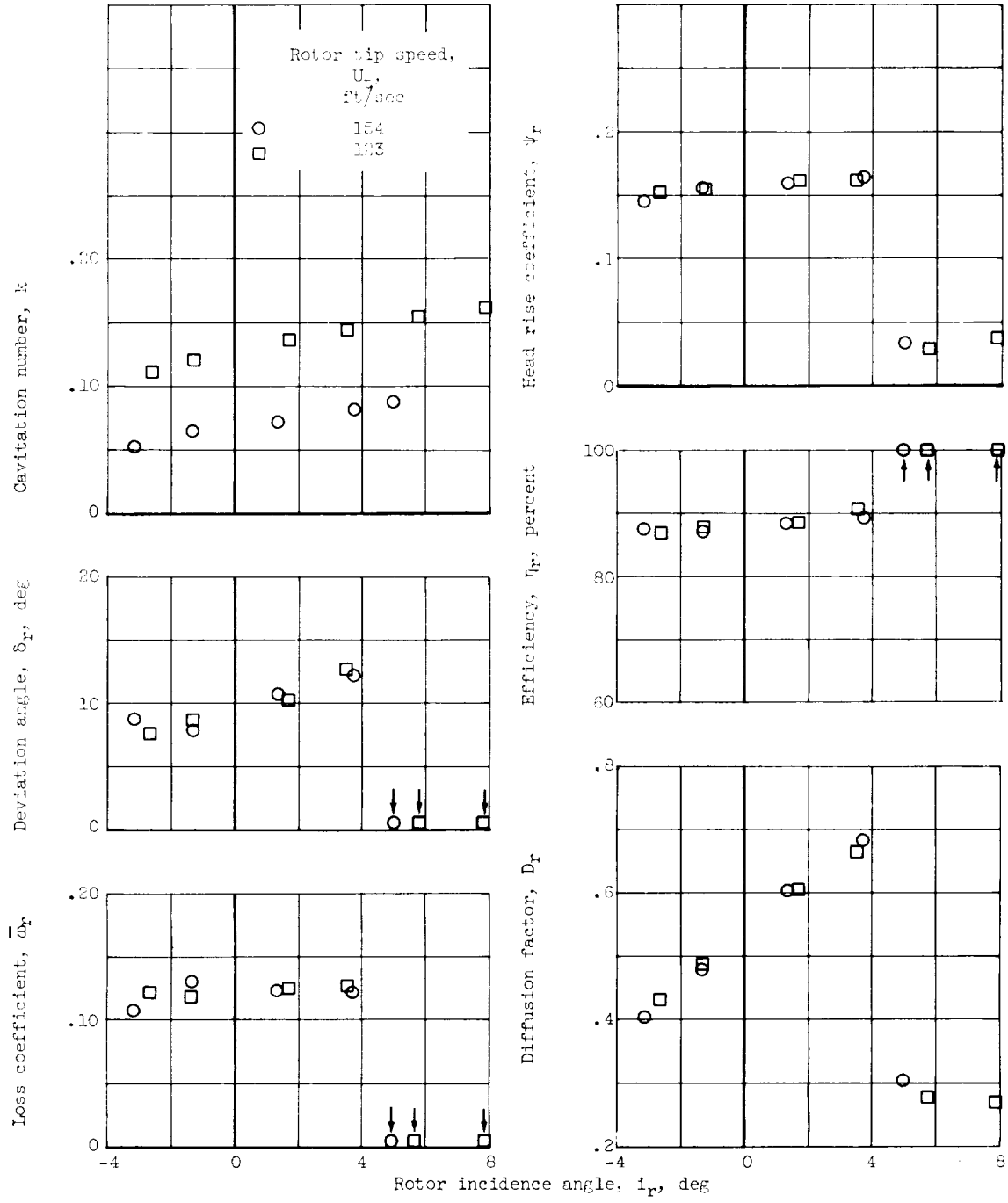

(e) 90 Percent passage height from tip.

Figure 11. - Concluded. Rotor blade-element characteristics (noncavitating). Suction head, 115 feet.

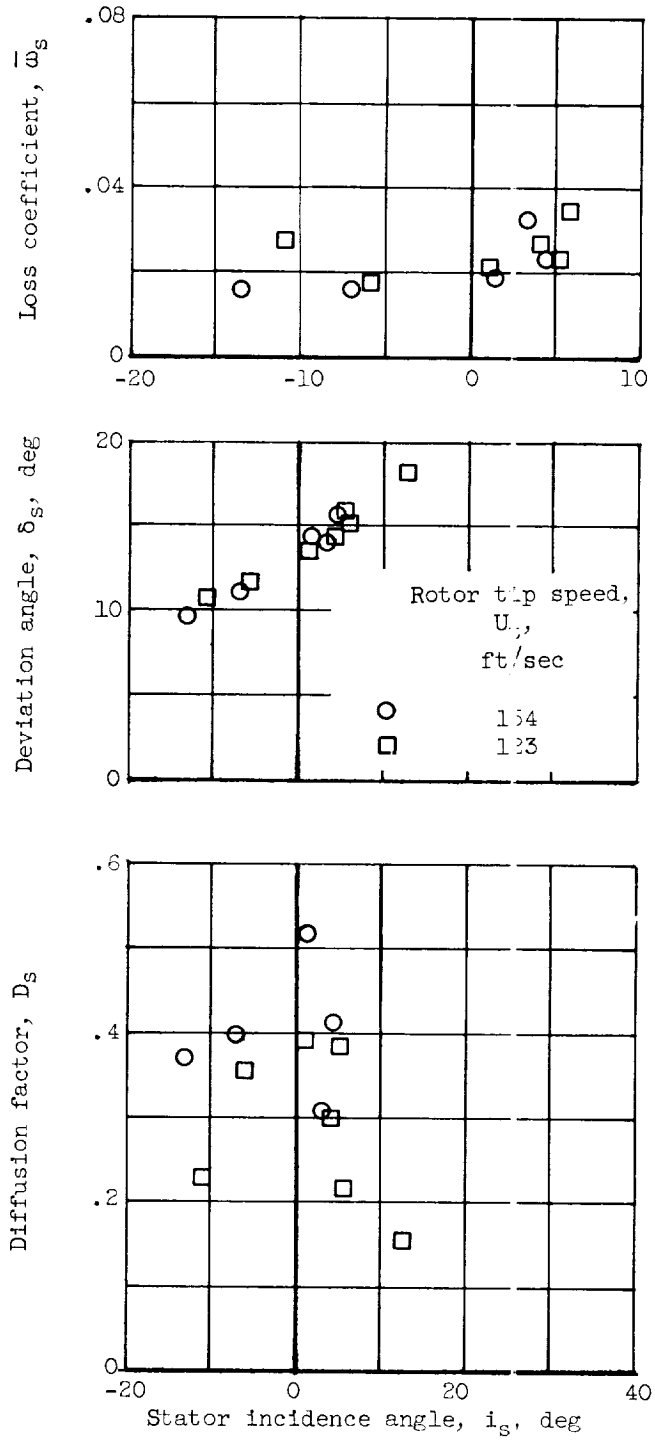

(a) 10 Percent passage height from tip.

Figure 12. - Stator blade-element data when the rotor is not cavitating. Suction head, 115 feet.

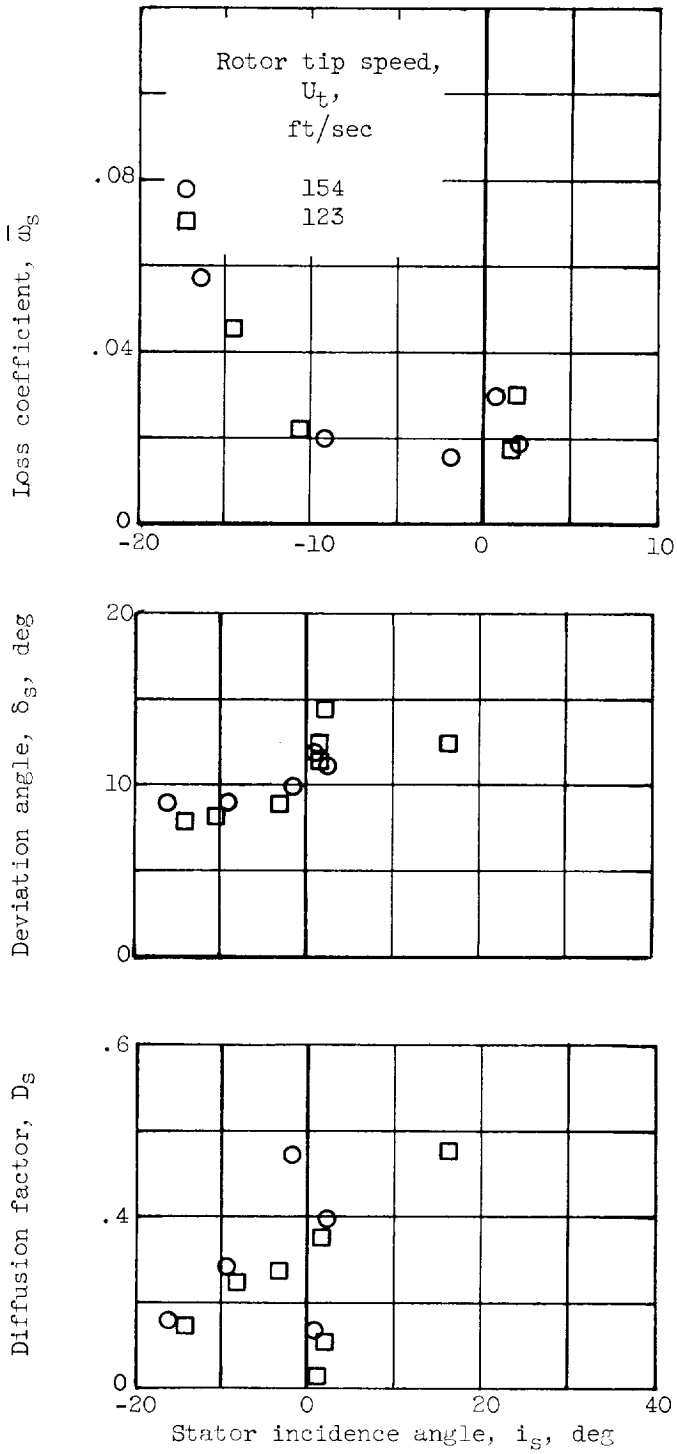

(b) 30 Percent passage height from tip.

Figure 12. - Continued. Stator blade-element data when the rotor is not cavitating. Suction head, 115 feet.

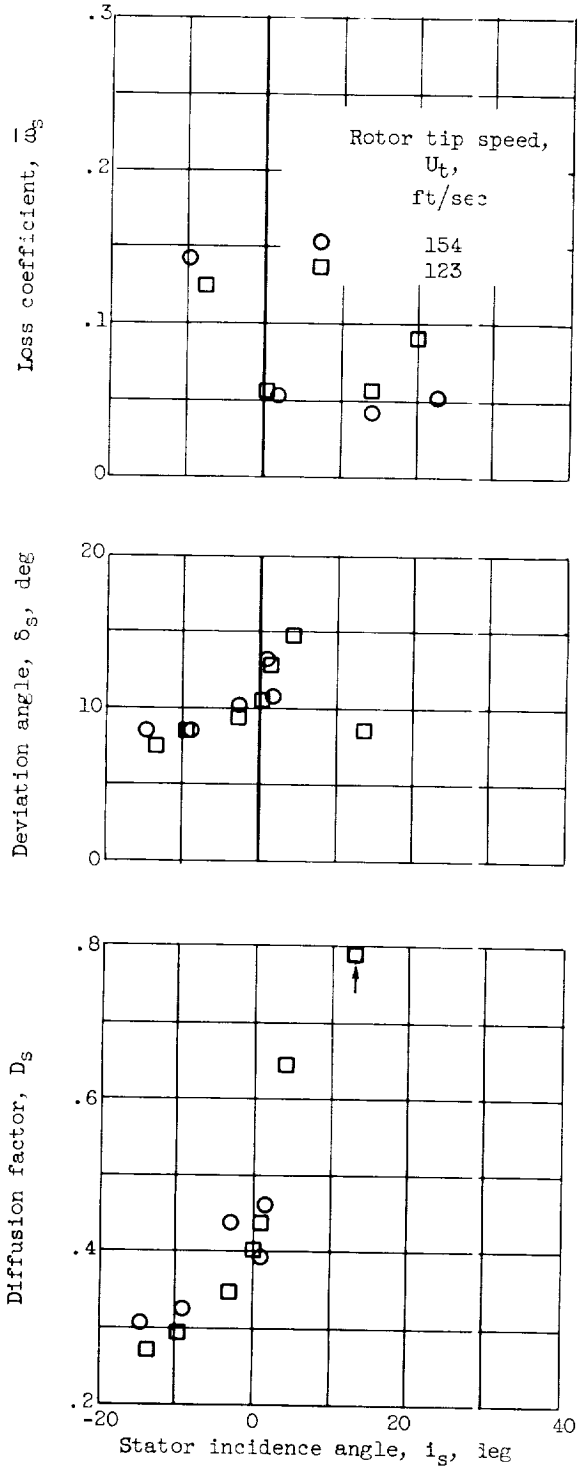

(c) 50 Percent passage height from tip.

Figure 12. - Continued. Stator blade-element data when the rotor is not cavitating. Suction head, 115 feet.

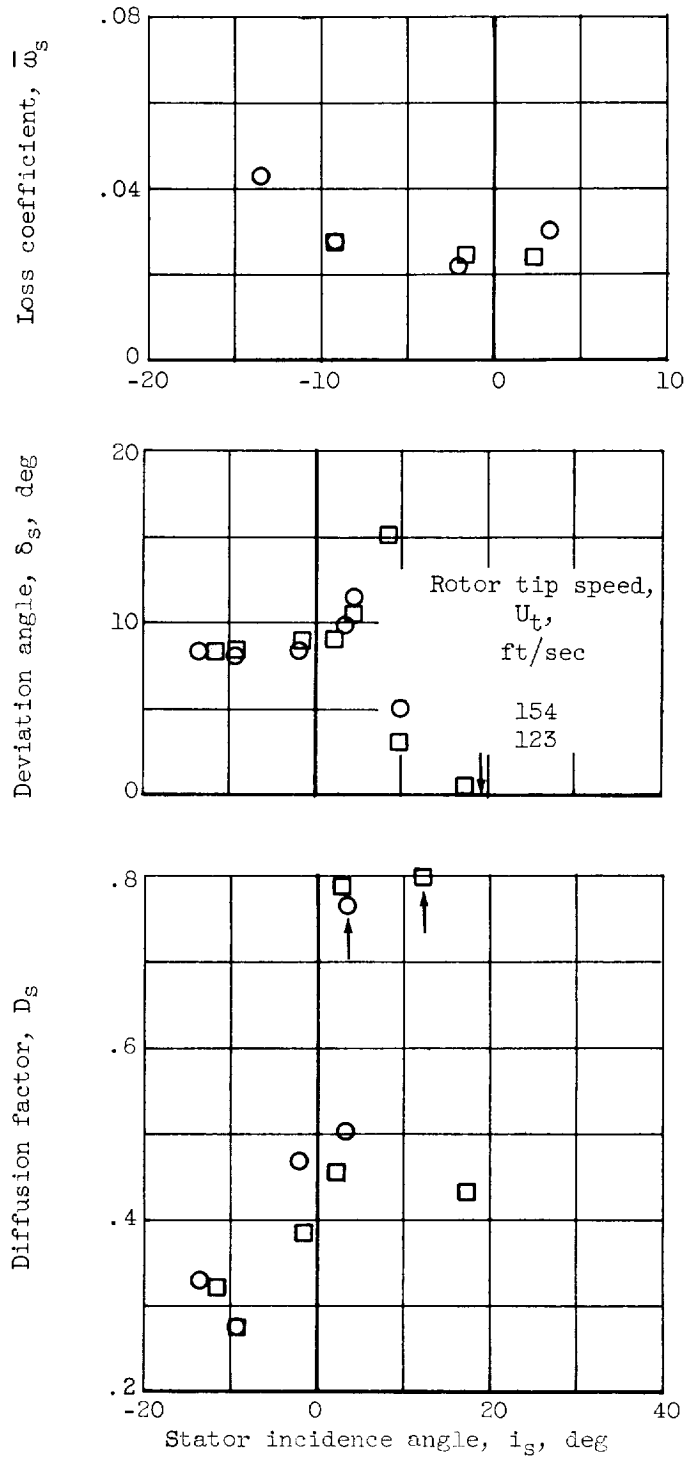

(d) 70 Percent passage height from tip.

Figure 12. - Continued. Stator blade-element data when the rotor is not cavitating. Suction head, 115 feet.

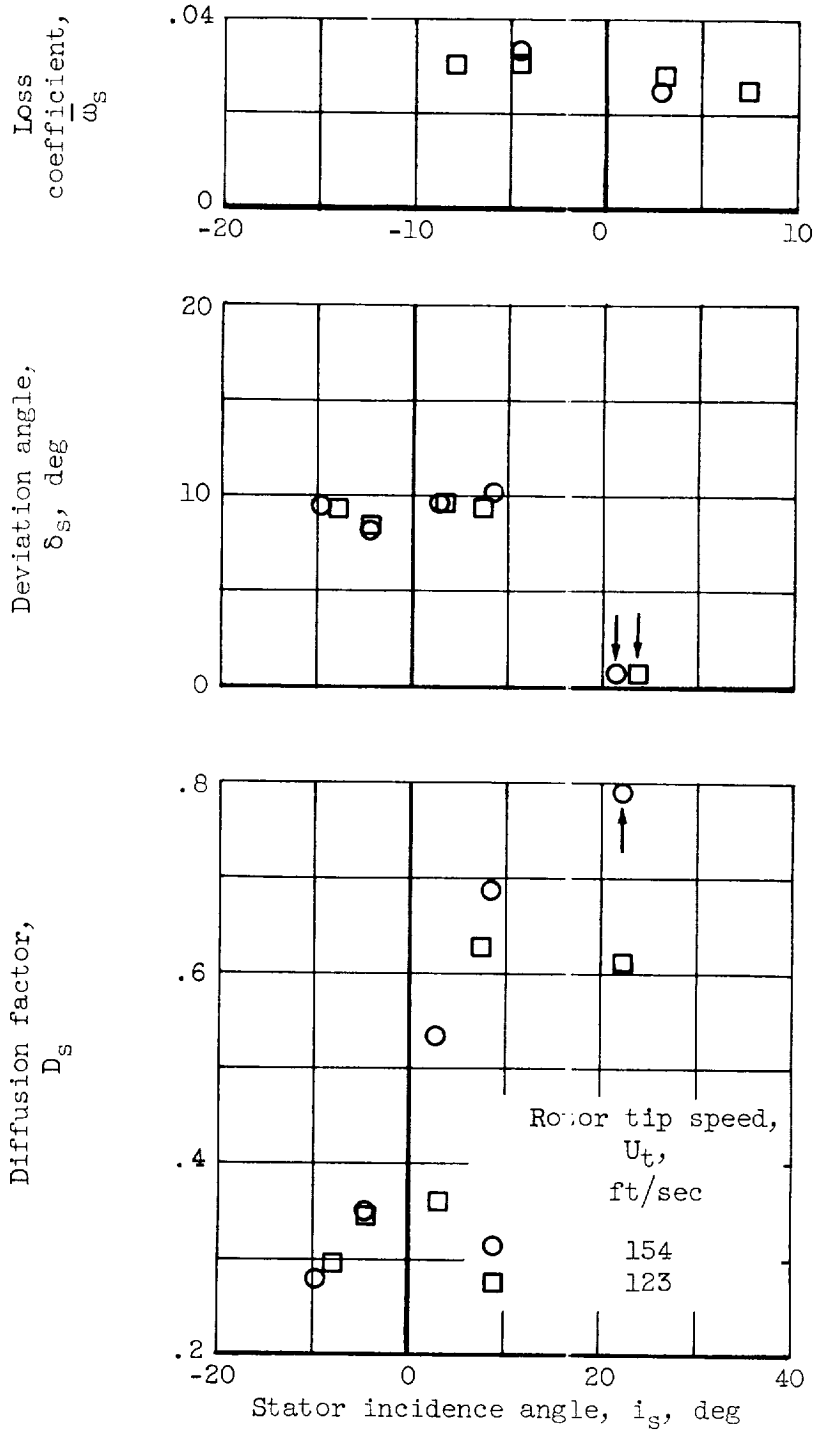

(e) 90 Percent passage height from tip.

Figure 12. - Concluded. Stator blade-element data when the rotor is not cavitating. Suction head, 115 feet.

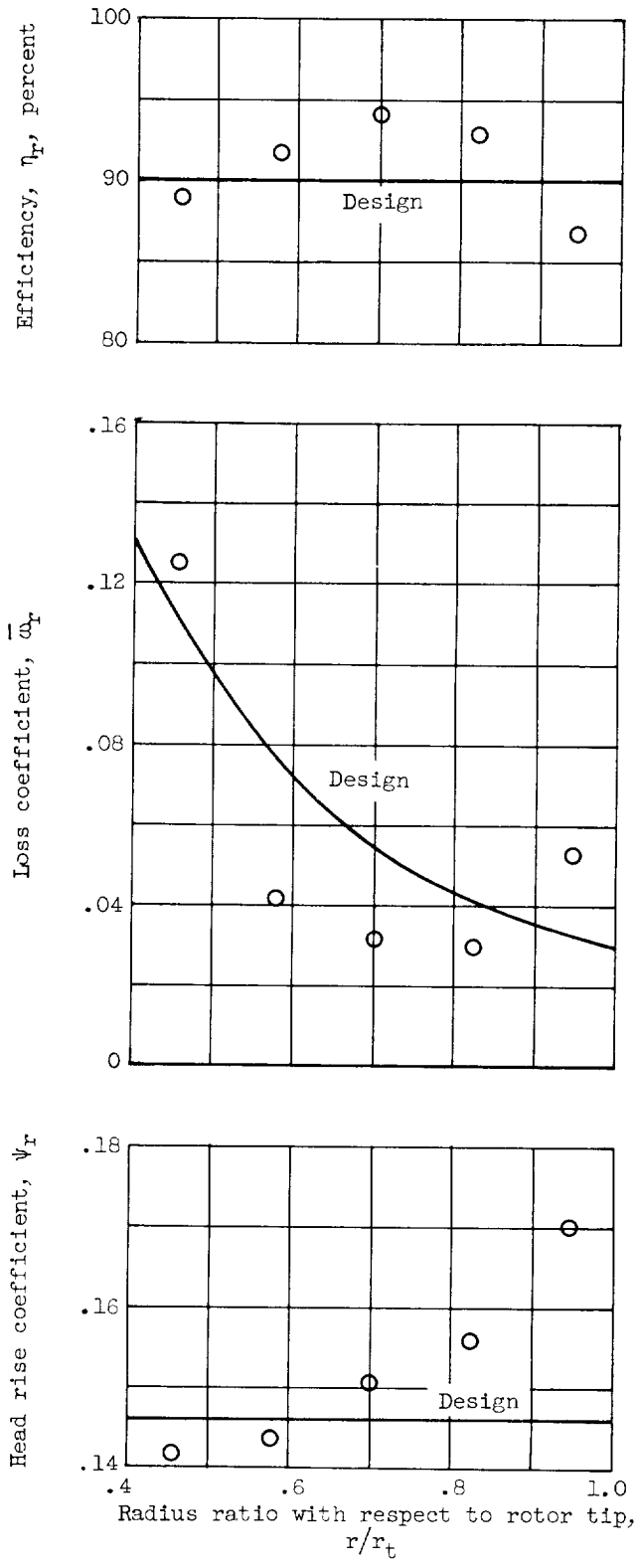

Figure 13. - Estimated rotor performance.

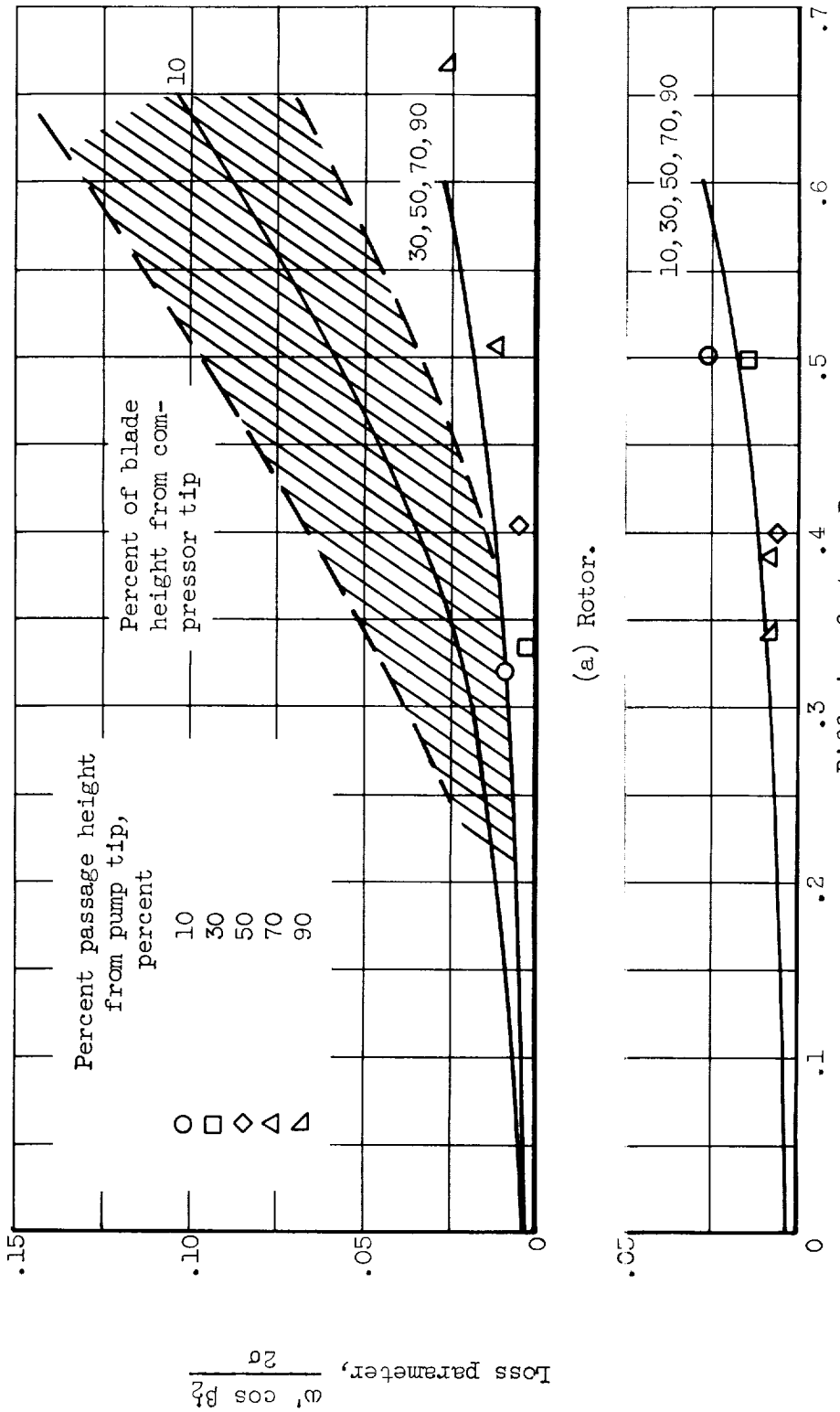

Figure 14. - Comparison of measured axial-flow pump results at reference minimum-loss incidence angle with corrections of reference 2.

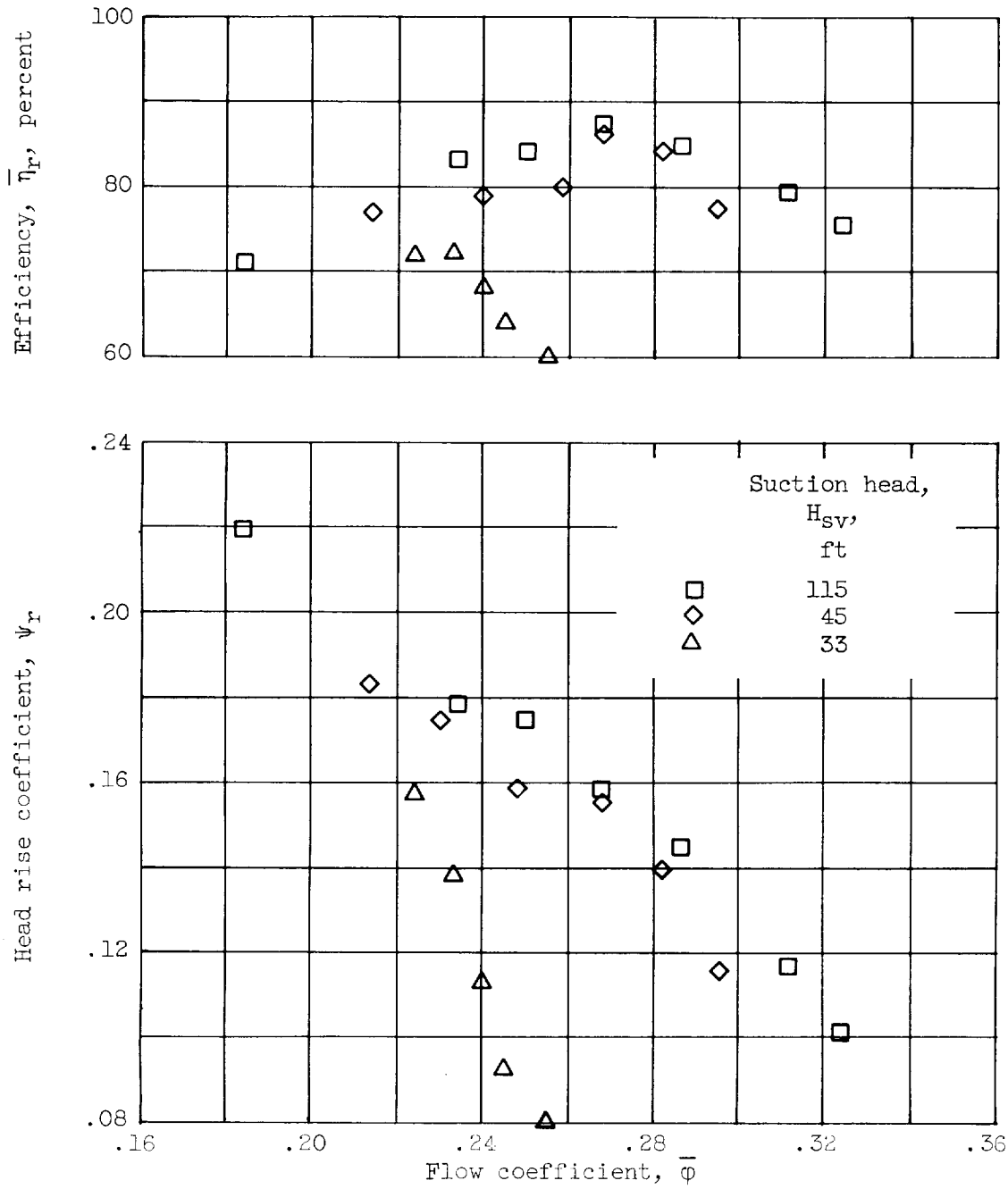

Figure 15. - Comparison of overall rotor performance at various net positive suction heads. Rotor tip speed, 123 feet per second.

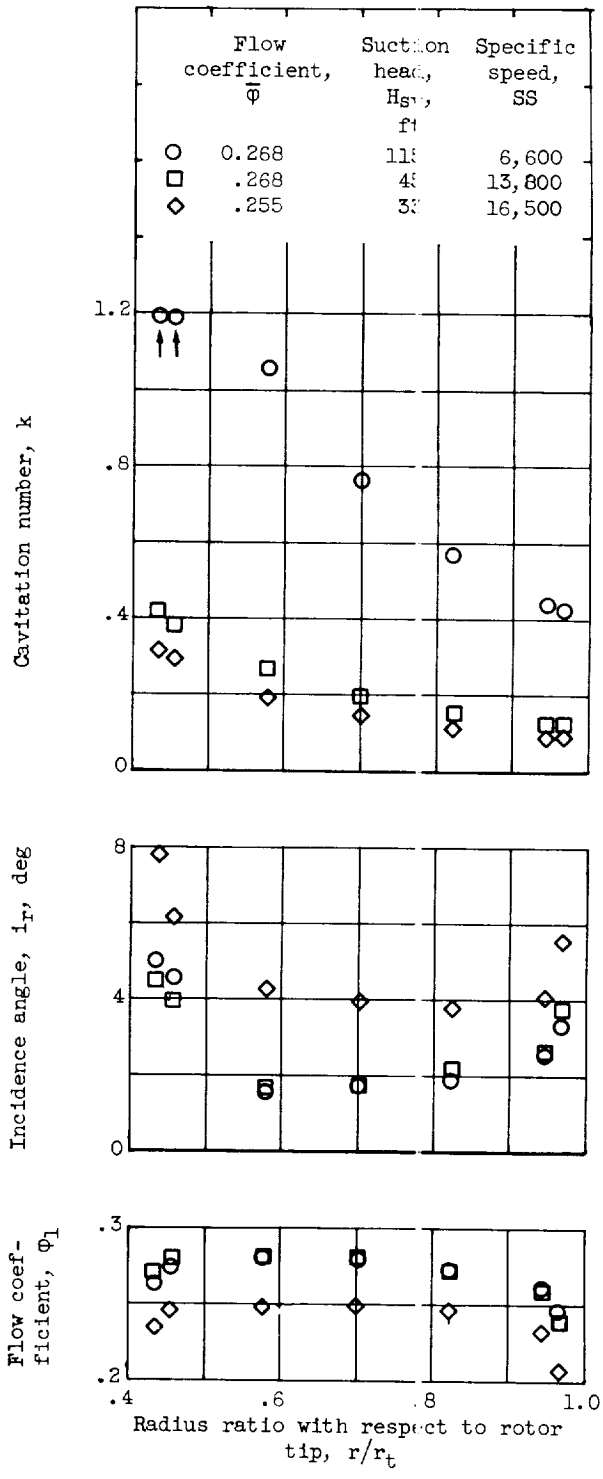

Figure 16. - Radial distributions of flow and blade-element parameters at rotor inlet for various net positive suction heads. Rotor tip speed, 123 feet per second.

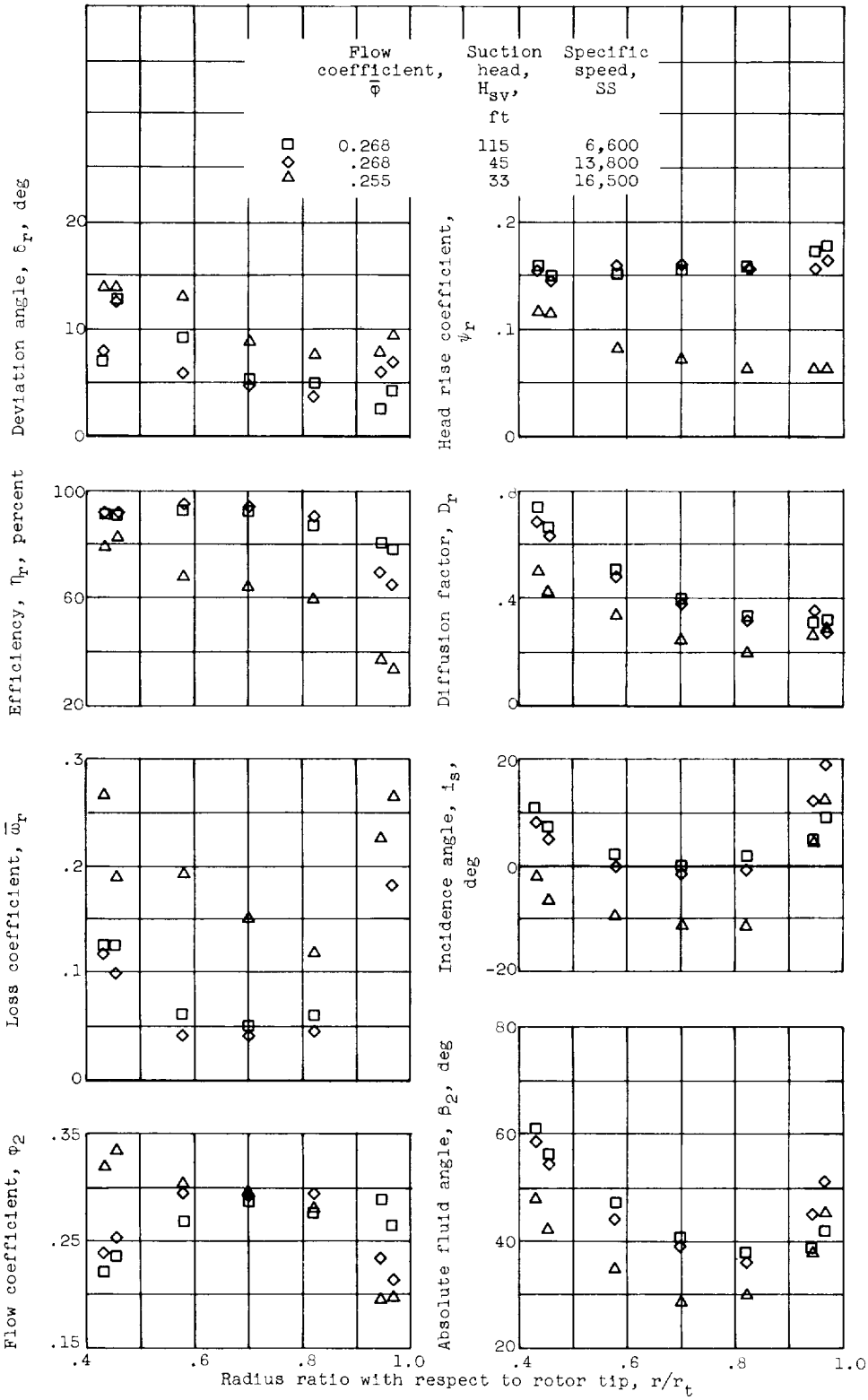

Figure 17. - Radial distributions of flow and blade-element parameters at rotor outlet (stator inlet) at various net positive suction heads. Rotor tip speed, 123 feet per second.

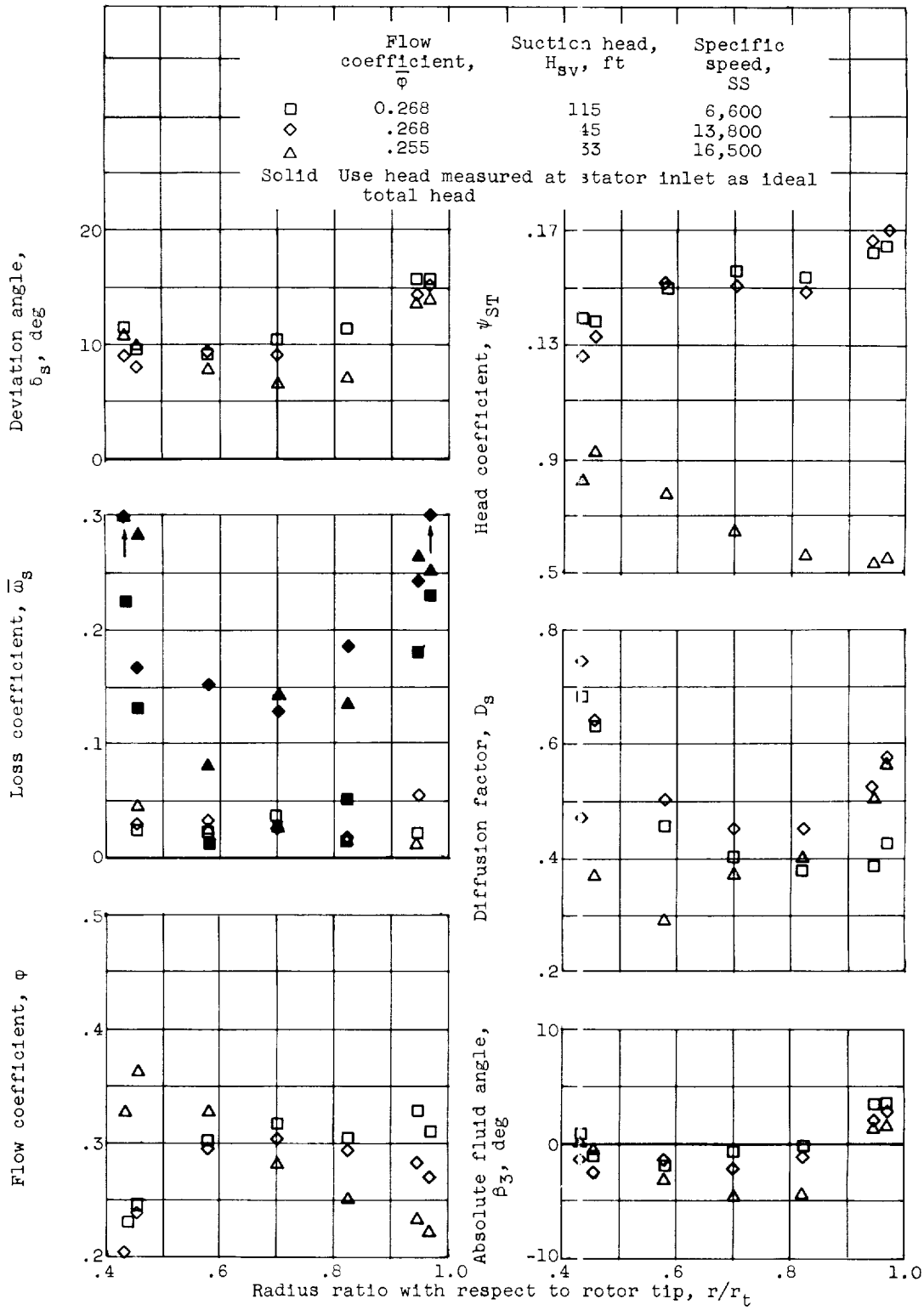

Figure 18. - Radial distributions of flows and blade-element parameters at stator outlet at various net positive suction heads. Rotor tip speed, 123 feet per second.

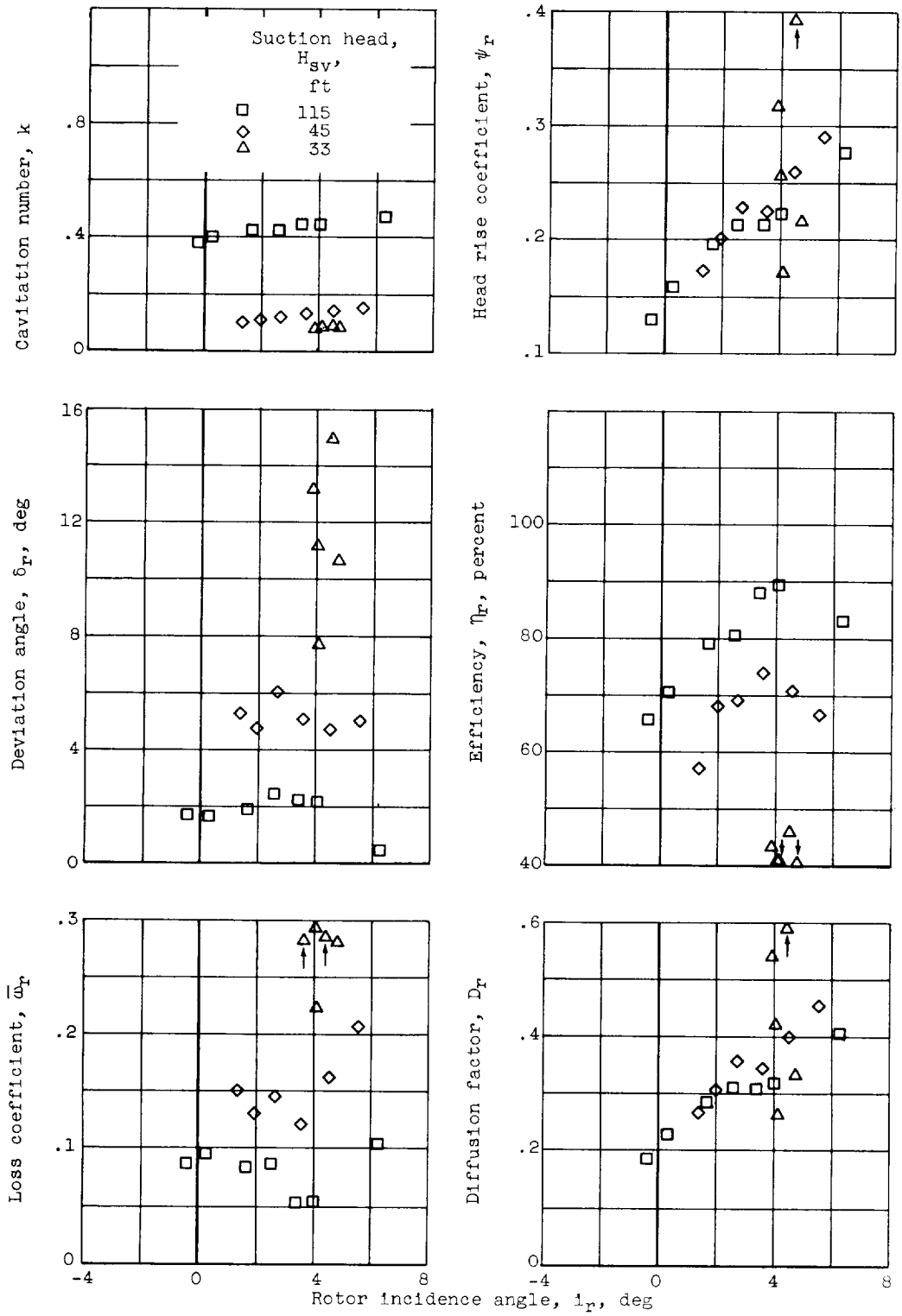

(a) 10 Percent passage height from tip.

Figure 19. - Rotor blade-element characteristics for various net positive suction heads. Rotor tip speed, 123 feet per second.

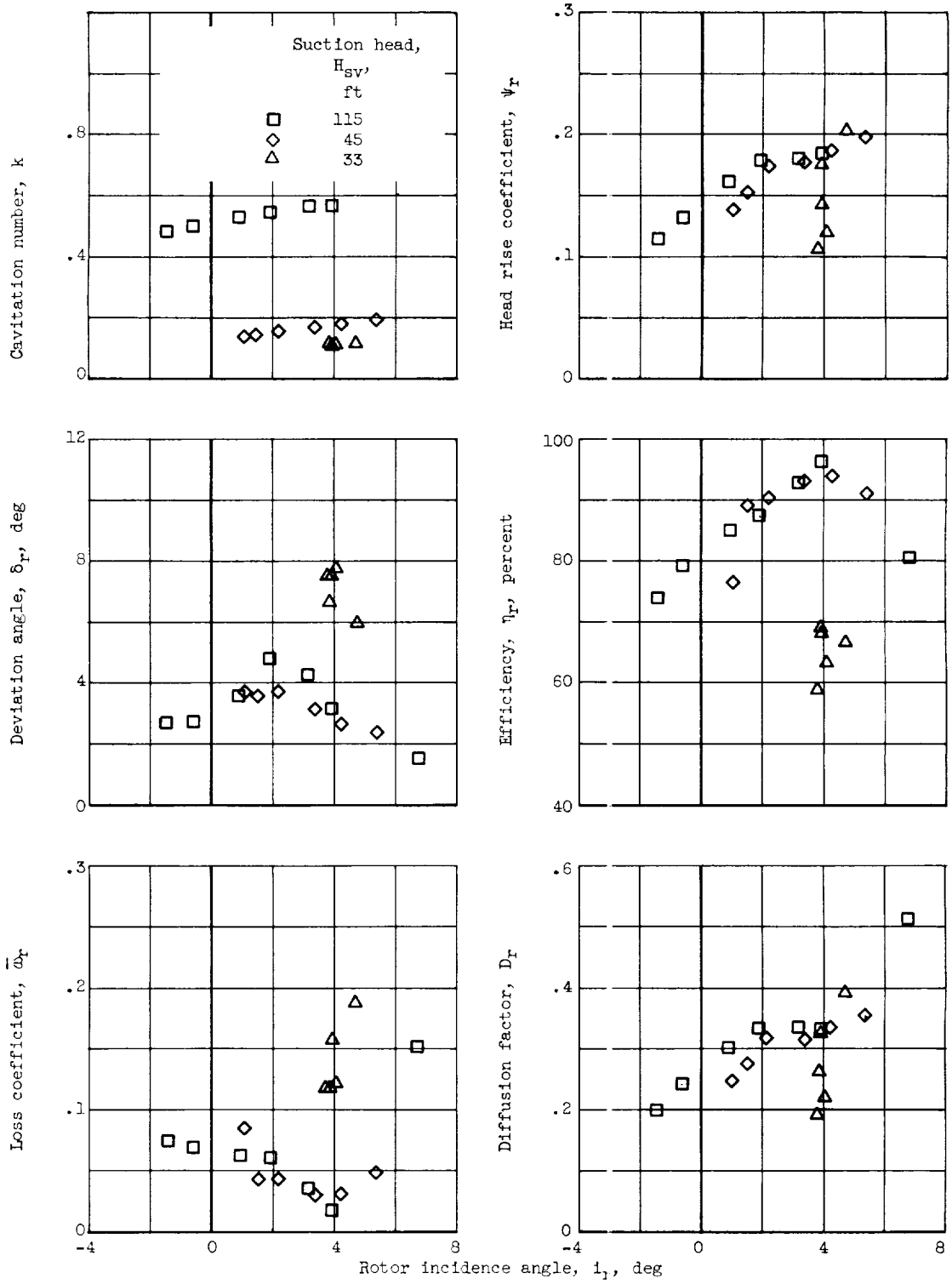

(b) 30 Percent passage height from tip.

Figure 19. - Continued. Rotor-blade-element characteristics for various net positive suction heads. Rotor tip speed, 123 feet per second.

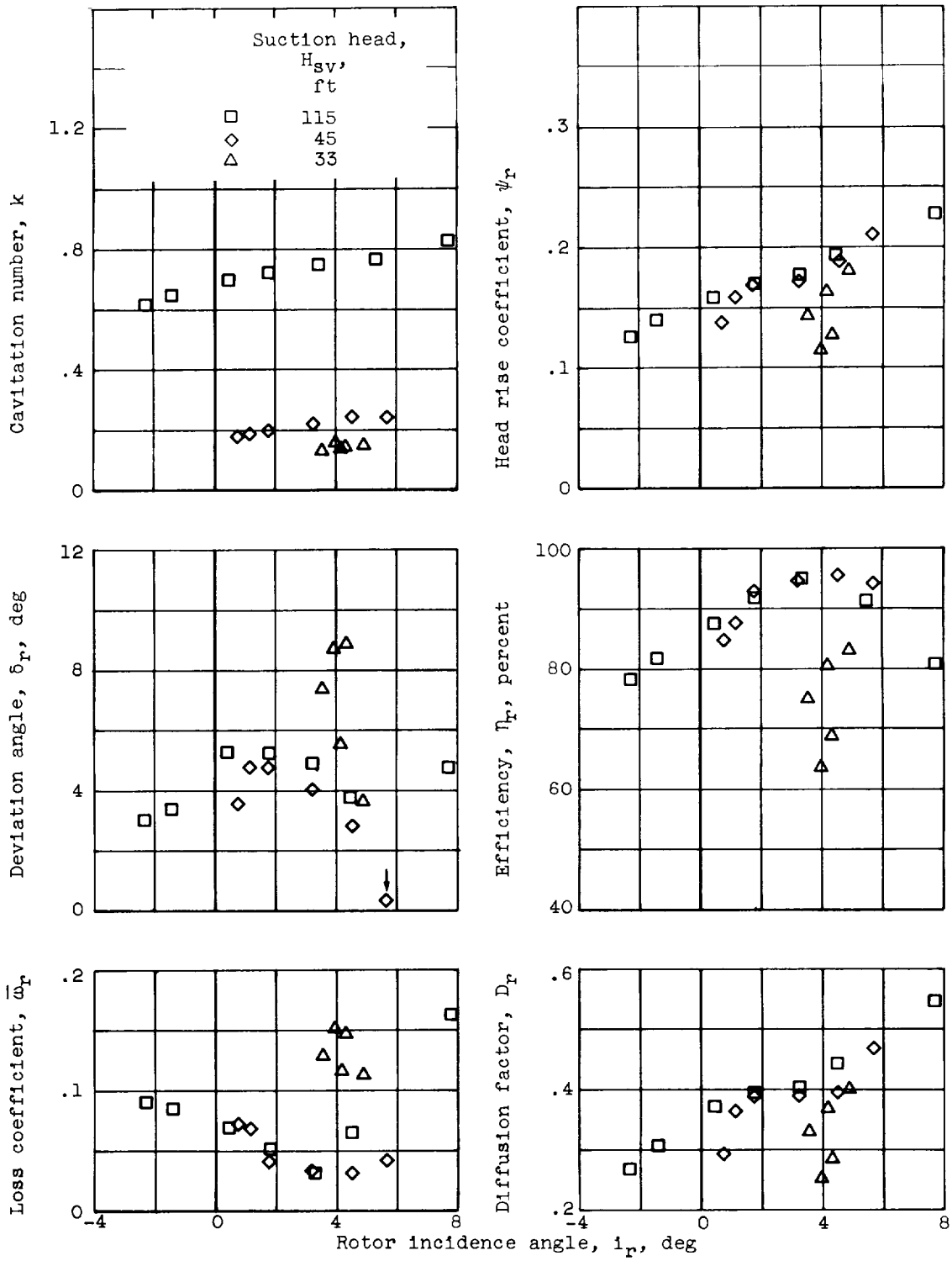

(c) 50 Percent passage height from tip.

Figure 19. - Continued. Rotor-blade-element characteristics for various net positive suction heads. Rotor tip speed, 123 feet per second.

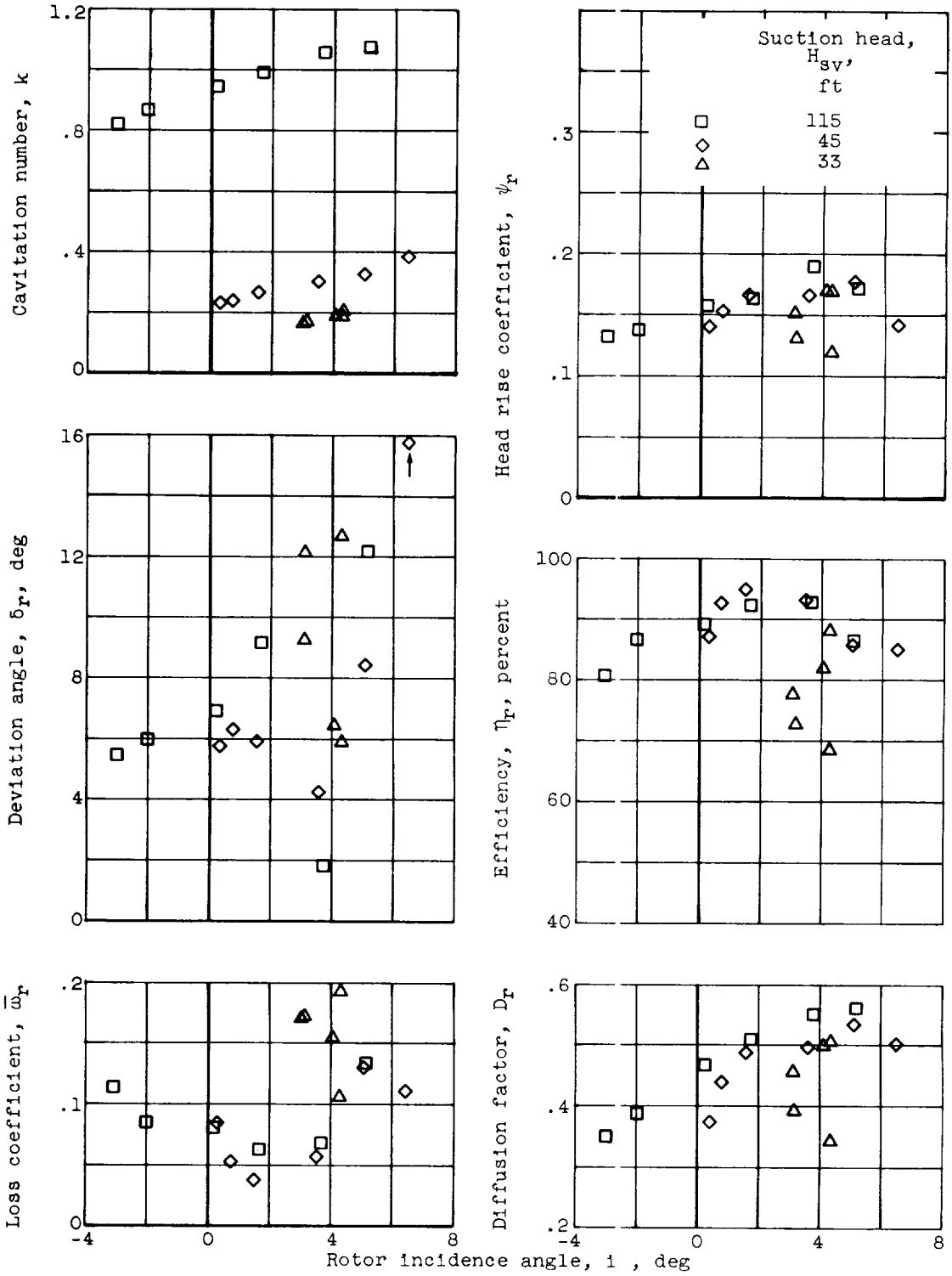

(d) 70 Percent passage height from tip.

Figure 19. - Continued. Rotor-blade-element characteristics for various net positive suction heads. Rotor tip speed, 123 feet per second.

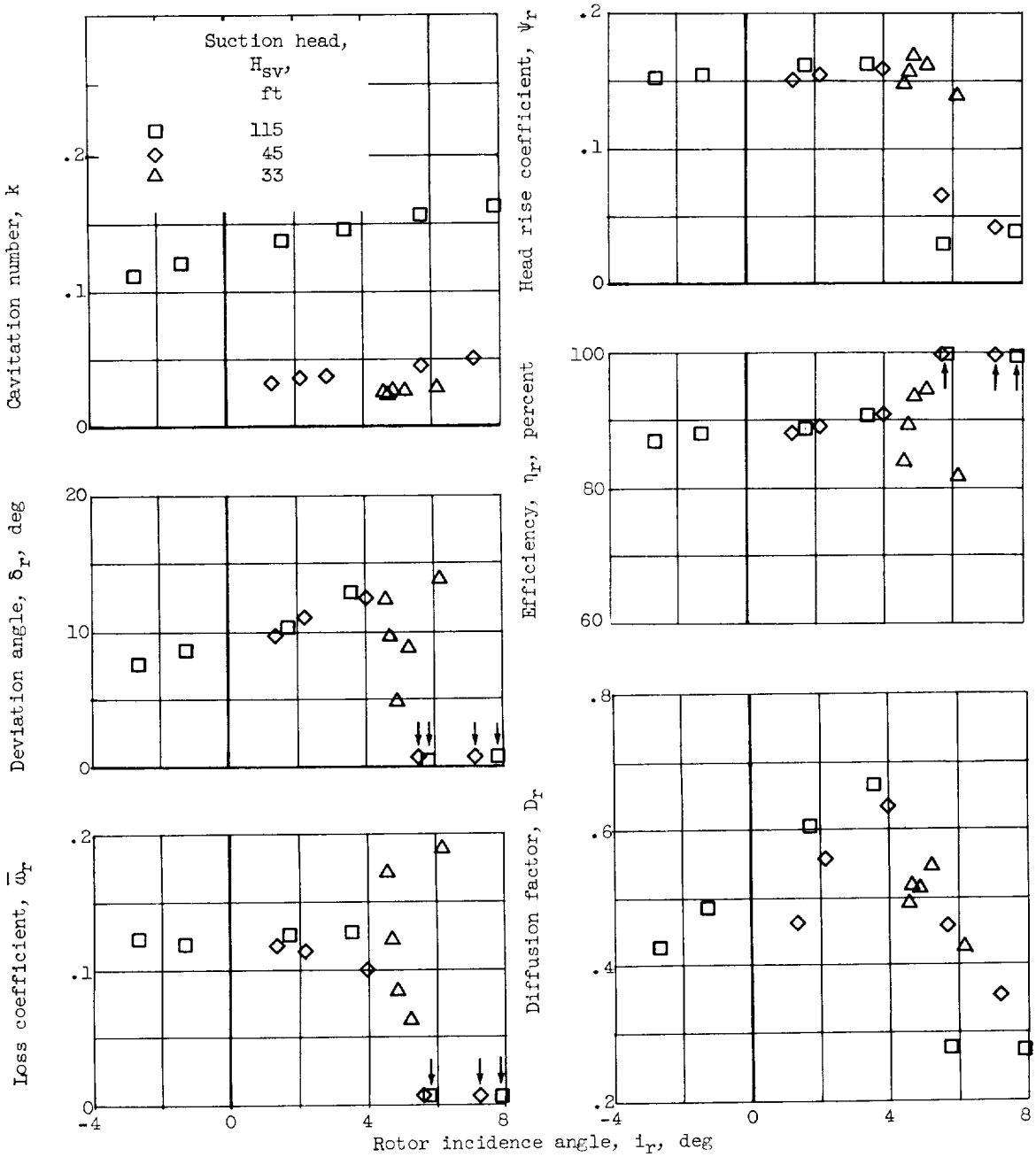

(e) 90 Percent passage height from tip.

Figure 19. - Concluded. Rotor-blade-element characteristics for various net positive suction heads. Rotor tip speed, 123 feet per second.

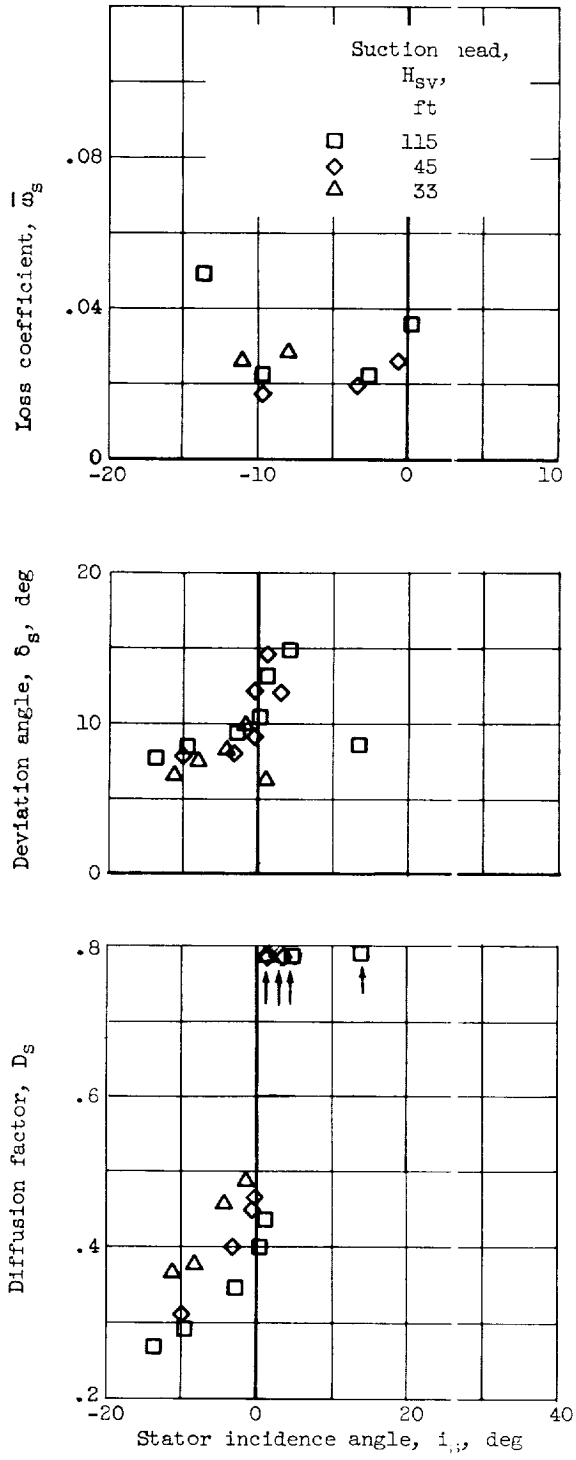

(c) 50 Percent passage height from tip.

Figure 20. - Continued. Stator-blade-element characteristics for various net positive suction heads. Rotor tip speed, 123 feet per second.

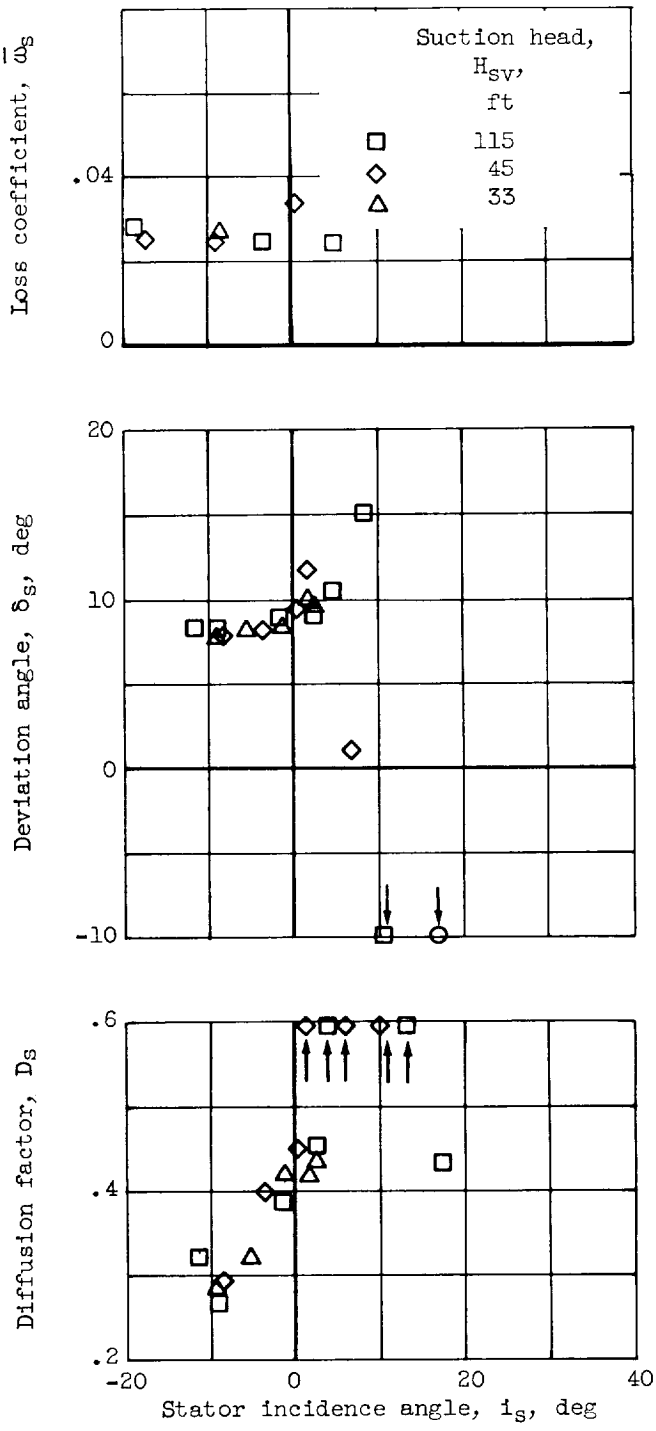

(d) 70 Percent passage height from tip.

Figure 20. - Continued. Stator-blade-element characteristics for various net positive suction heads. Rotor tip speed, 123 feet per second.

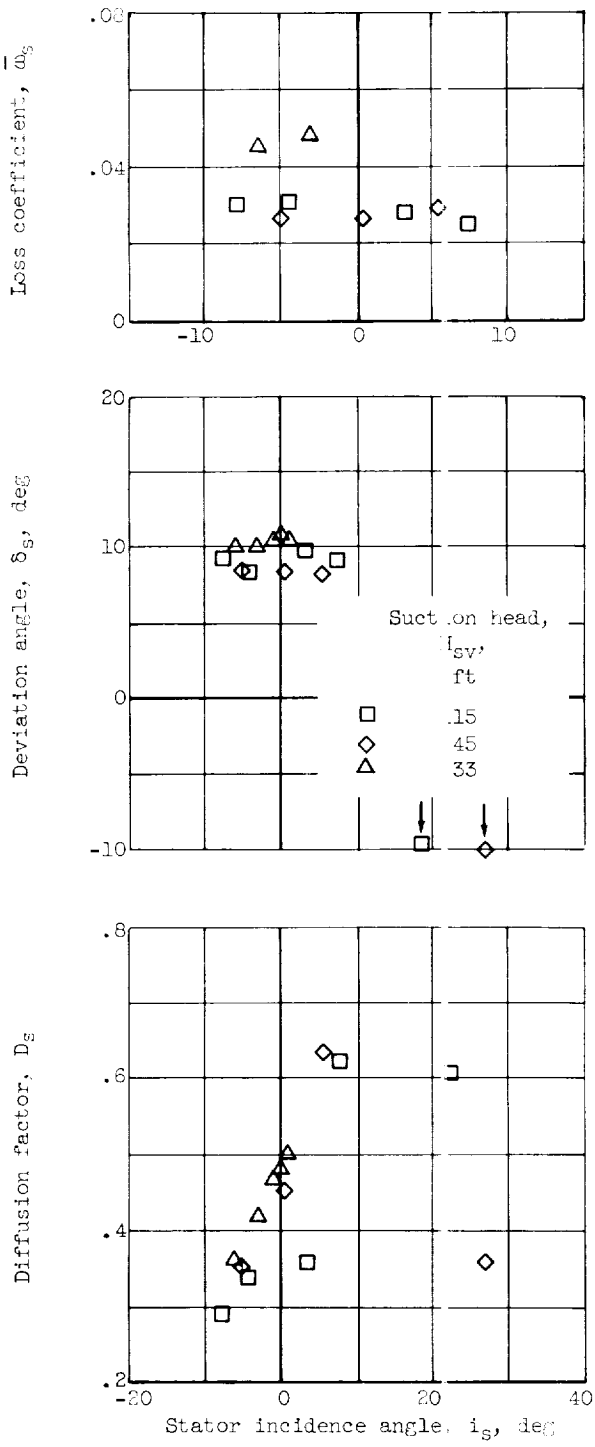

(e) 90 Percent passage height from tip.

Figure 20. - Concluded. Stator-blade-element characteristics for various net positive suction heads. Rotor tip speed. 123 feet per second.

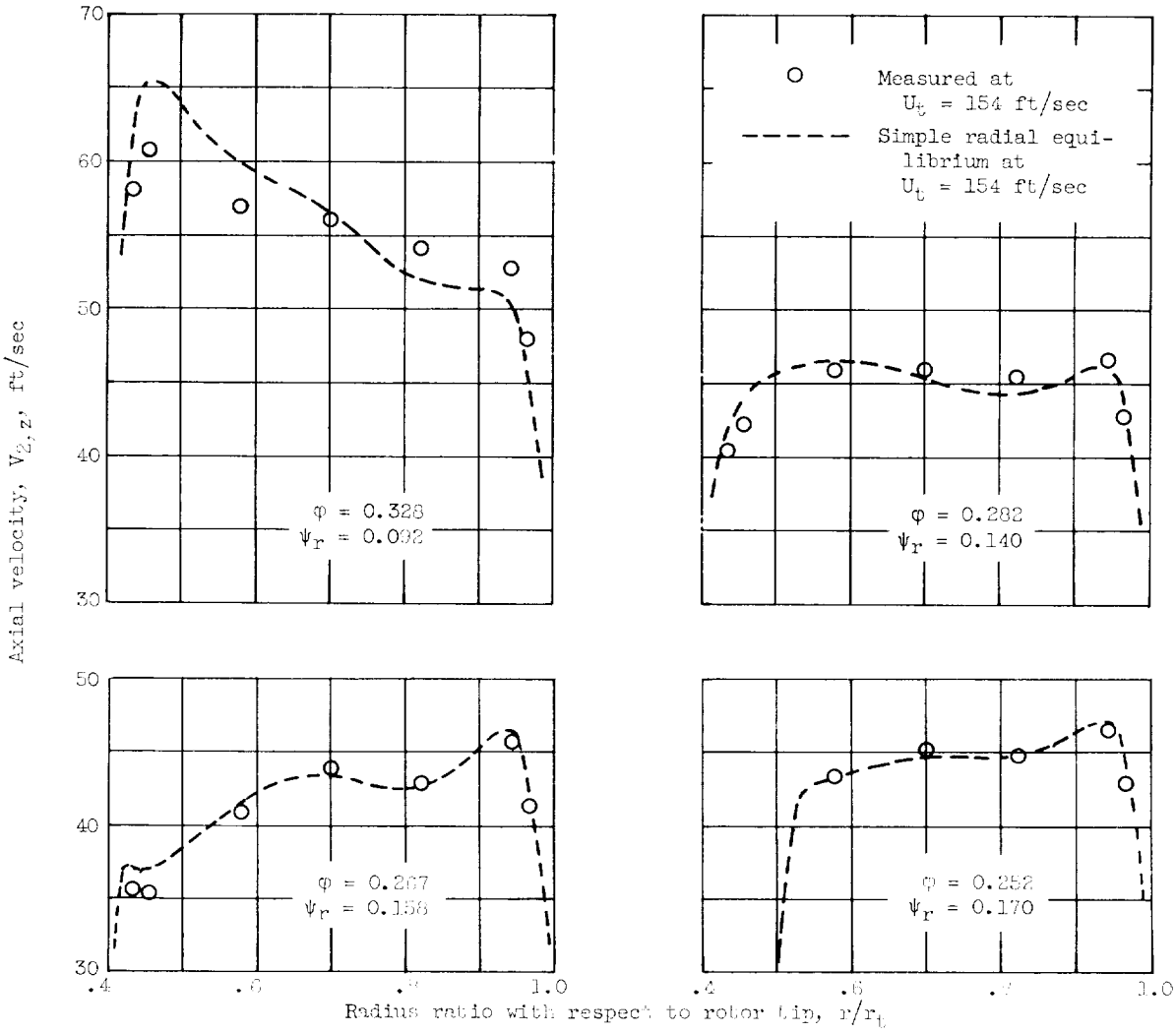

Figure 21. - Comparison of measured axial-velocity distribution behind rotor under noncavitating conditions with axial-velocity distribution behind rotor calculated by simple radial equilibrium. Suction head, 115 feet.

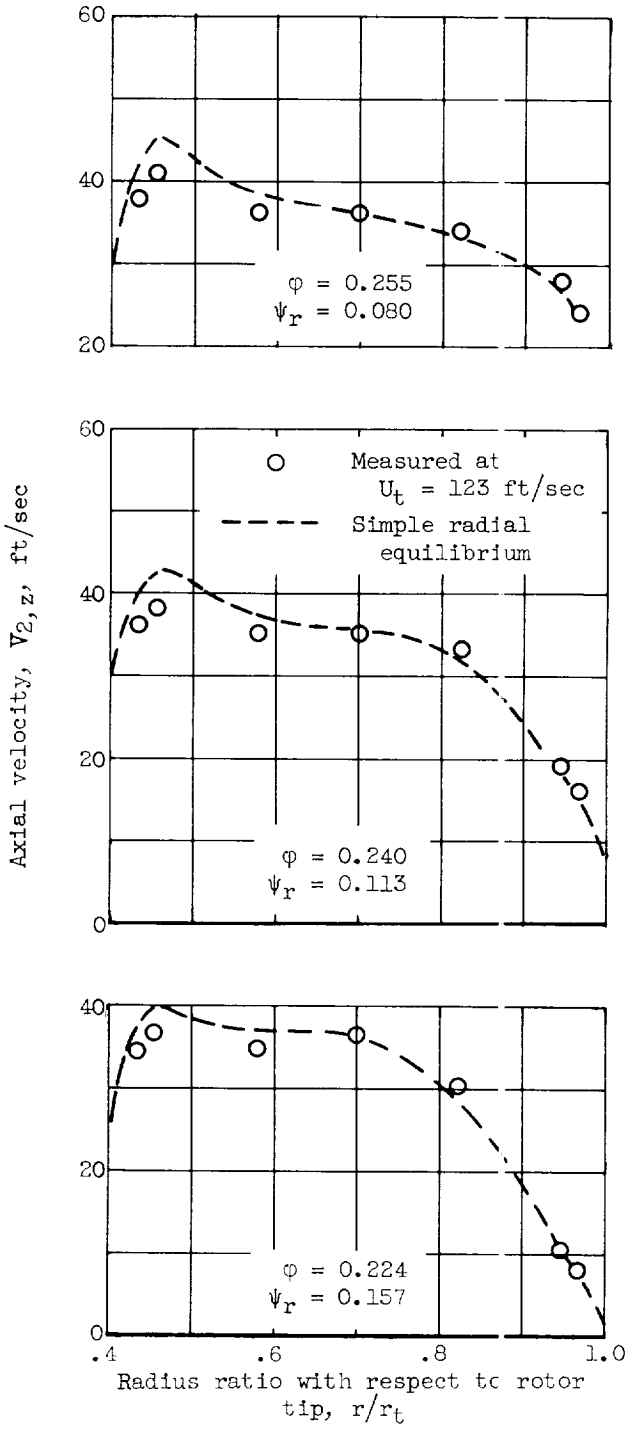

Figure 22. - Comparison of measured axial-velocity distribution behind rotor under cavitating conditions with the axial-velocity distribution behind rotor calculated by simple radial equilibrium. Suction head, 33 feet.